Proteomic profiling reveals distinct phases to the restoration of chromatin following DNA replication

Alvarez, Vanesa; Bandau, Susanne; Jiang, Hao; Rios-Szwed, Diana; Hukelmann, Jens; Garcia-Wilson, Elisa

Published in:
Cell Reports

DOI:
10.1016/j.celrep.2023.111996

Publication date:
2023

Cell Reports

Resource

Proteomic profiling reveals distinct phases to the restoration of chromatin following DNA replication

Graphical abstract

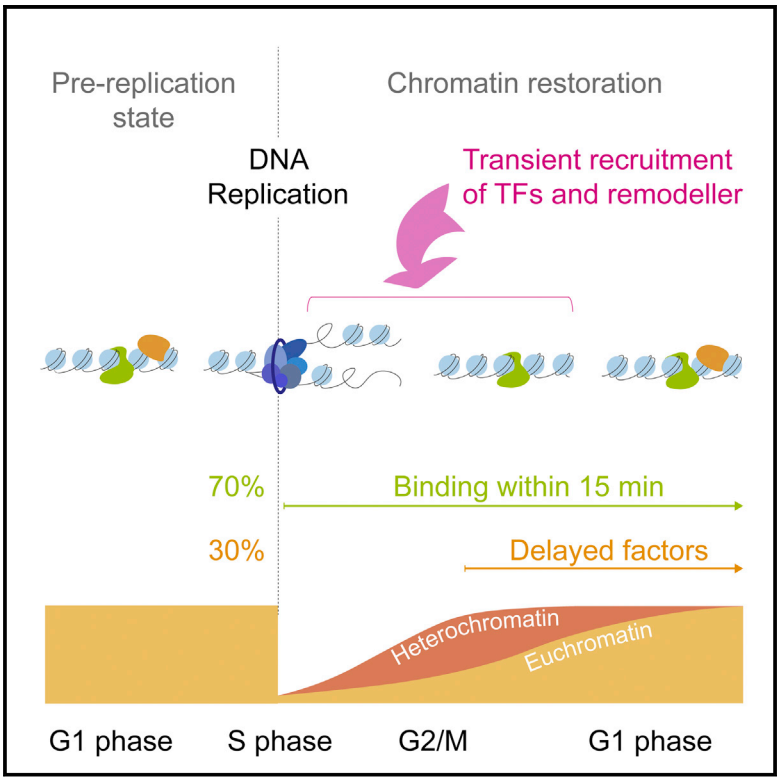

Authors

Vanesa Alvarez, Susanne Bandau, Hao Jiang, ..., Tom Owen-Hughes, Angus Lamond, Constance Alabert

Correspondence

calabert@dundee.ac.uk

In brief

Using quantitative proteomics coupled to replicated chromatin isolation, Alvarez et al. investigate how chromatin proteins reassociate with newly replicated DNA. They show that DNA replication disrupts but also promotes the recruitment of thousands of proteins, providing a resource to understand how chromatin-based information is maintained through rounds of cell division.

Highlights

- Behind replisomes, most chromatin proteins reassociate within minutes
- Chromatin restoration is completed after mitosis, in the daughter cells
- Heterochromatin is more propitious to restoration than euchromatin
- Newly replicated chromatin contains an excess of selected transcription factors

Alvarez et al., 2023, Cell Reports *42*, 111996
January 31, 2023
https://doi.org/10.1016/j.celrep.2023.111996

CellPress

Cell Reports

CellPress
OPEN ACCESS

Resource

Proteomic profiling reveals distinct phases to the restoration of chromatin following DNA replication

Vanesa Alvarez,[1] Susanne Bandau,[1] Hao Jiang,[2] Diana Rios-Szwed,[1,4] Jens Hukelmann,[2] Elisa Garcia-Wilson,[1] Nicola Wiechens,[3] Eva Griesser,[2] Sara Ten Have,[2] Tom Owen-Hughes,[3] Angus Lamond,[2] and Constance Alabert[1,5,*]

[1]Division of Molecular, Cell, and Developmental Biology, School of Life Sciences, University of Dundee, Dundee DD1 5EH, Scotland, UK
[2]Laboratory of Quantitative Proteomics, Division of Molecular, Cell, and Developmental Biology, School of Life Sciences, University of Dundee, Dundee DD1 5EH, Scotland, UK
[3]Laboratory of Chromatin Remodelling and Cancer Epigenetics, Division of Molecular, Cell & Developmental Biology, School of Life Sciences, University of Dundee, Dundee DD1 5EH, Scotland, UK
[4]Present address: MRC Human Genetics Unit, Edinburgh EH4 2XU, Scotland, UK
[5]Lead contact
*Correspondence: calabert@dundee.ac.uk
https://doi.org/10.1016/j.celrep.2023.111996

SUMMARY

Chromatin organization must be maintained during cell proliferation to preserve cellular identity and genome integrity. However, DNA replication results in transient displacement of DNA-bound proteins, and it is unclear how they regain access to newly replicated DNA. Using quantitative proteomics coupled to Nascent Chromatin Capture or isolation of Proteins on Nascent DNA, we provide time-resolved binding kinetics for thousands of proteins behind replisomes within euchromatin and heterochromatin in human cells. This shows that most proteins regain access within minutes to newly replicated DNA. In contrast, 25% of the identified proteins do not, and this delay cannot be inferred from their known function or nuclear abundance. Instead, chromatin organization and G1 phase entry affect their reassociation. Finally, DNA replication not only disrupts but also promotes recruitment of transcription factors and chromatin remodelers, providing a significant advance in understanding how DNA replication could contribute to programmed changes of cell memory.

INTRODUCTION

Chromatin organization is instrumental for genome function and stability. In S phase, chromatin is challenged by the progression of thousands of replisomes, provoking a genome-wide disassembly of nucleosomes ahead of the fork and their reassembly behind.[1–3] Understanding how chromatin-encoded information is faithfully re-established on the two daughter strands is a central question in the fields of gene regulation and cell fate and provides insight into how perturbations may lead to pathological outcomes.[4–6]

Behind replisomes, nucleosomes are assembled within minutes with no defined spacing, using a mix of recycled parental and newly synthesized histones. This results in a transient loss of transcription factor (TF) access to newly replicated DNA.[7,8] Moreover, parental histones retain post translational modifications (PTMs) while newly synthesized histones are di-acetylated on histone H4 lysine 5 and 12.[9] This leads to a transient dilution of pre-existing histone PTMs and an increase of histone acetylation on newly replicated chromatin.[10] Within 2 hours, nucleosome positioning is regained, TF accessibility is restored, and transcription restarts.[8] However, not all chromatin components have been re-established on newly replicated DNA. For instance, the re-establishment of H3K27me3 and the incorporation of the centromeric histone variant CENP-A are completed after mitosis.[10–12]

Mechanistically, the production of two daughter strands from one parental strand represents two challenges. First, locus-specific components need to regain access to the pre-replication genomic position. Several mechanisms, not necessarily tightly coupled to DNA replication, have been proposed to ensure site-specific maintenance of chromatin state such as the H3K9me3 self-enforcing loop.[13] Second, twice the amount of protein is needed to faithfully reconstitute chromatin on the two daughter strands from one parental strand. For histones, the challenge of doubling the number of nucleosomes is overcome by (1) the recycling of histones from parental strands to the two daughter strands,[3] and (2) synthesis of new histones in S phase.[14] How other chromatin components are duplicated on the two sister chromatids remains unclear.

To investigate how chromatin components reassemble following DNA replication, previous studies have used either chromatin immunoprecipitation in synchronized cells,[15] or imaging,[11,16] focusing on the analysis of selected proteins and selected sites. More recently, technologies based on the labeling of newly replicated DNA are used to monitor the composition of nascent chromatin.[2,8,17,18] These studies focused on the first 2 h after the

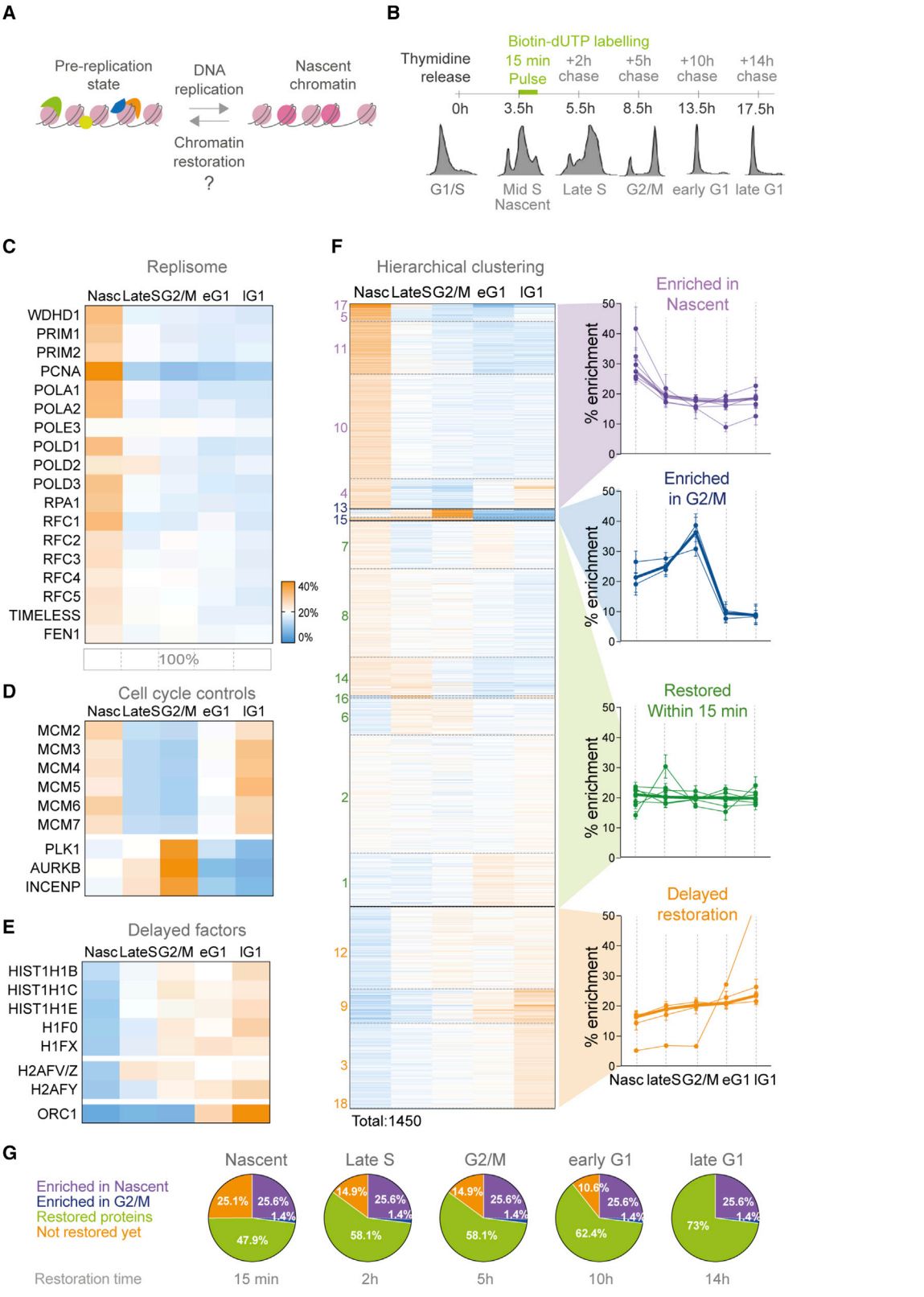

(legend on next page)

passage of the fork or on histone modifications.[10] As it is often a combination of several chromatin features that ensure faithful inheritance of silenced and active states, it thus remains unresolved how chromatin is faithfully duplicated on newly replicated DNA. Here, we tracked the composition of chromatin at successive time points, ranging from 15 min following its assembly on newly replicated DNA, to 14 h in the subsequent G1 phase. To this end, we combined Nascent Chromatin Capture (NCC)[17] or isolation of Proteins On Nascent DNA (iPOND)[19] with tandem mass tag (TMT) quantitative mass spectrometry.[20] The improved temporal resolution of the resulting data reveals that most proteins are restored within minutes after the passage of the fork. In contrast, for hundreds of proteins, their restoration is achieved several hours later, and varies between euchromatin and heterochromatin. Altogether, this time-resolved dataset provides a comprehensive picture of how chromatin components are restored over different time scales and different regions of the genome to allow transmission of chromatin-based information through cell divisions.

RESULTS

Proteomic profiling of replicated chromatin from S phase to the subsequent G1 phase

To uncover how proteins regain access to newly replicated DNA, we monitored the composition of chromatin from its assembly behind replisomes to the subsequent G1 phase (Figures 1A and 1B). To this end, NCC was combined with TMT mass spectrometry in synchronized HeLa S3 cells. In mid-S phase, newly replicated DNA was biotin-dUTP labeled for 15 min and cells were collected immediately (15 min pulse, Nasc), 2 h later (Chase, Late S), 5 h later (Chase, G2/M), 10 h later (Chase, early G1), and 14 h later (Chase, late G1). Replicated chromatin was isolated by biotin purification, TMT labeled, and analyzed by mass spectrometry (Figure S1A). Cell cycle progression was monitored by flow cytometry (Figure 1B), six independent biological replicates performed (Figures S1B–S1D), and 5,770 proteins identified, of which 1,450 proteins were identified in all conditions (Table S1).

The relative abundances between time points were calculated for each protein and expressed as percentage in a heatmap format (Figure 1C). Core replisome components were enriched at the nascent time point compared with any later time points, indicating that nascent chromatin has been successfully isolated (Figures 1C and S1E). The abundance of mitotic factors such as PLK1, AURKA, and AURKB peaked onto replicated chromatin as cells reached G2/M (Figure 1D). Moreover, the MCM2-7 complex, which is part of the replisome and loaded *de novo* upon origin licensing in subsequent G1 phase,[21] showed, as expected, dual enrichment in Nascent and late G1 phase. This was confirmed by western blot analysis (Figure S1F) and together with flow cytometry, revealed that cell cycle synchronization was successful. Finally, proteins known to not regain immediate access to newly replicated DNA such as Histone H1,[9] histone variant H2A-Z,[10] or ORC1,[21] were low in abundance on nascent chromatin compared with later time points (Figure 1E). Altogether, these findings indicate that the experimental approach captured distinct phases in the maturation of nascent chromatin.

Hierarchical clustering reveals the behavior of specific protein groups

To capture the different phases of chromatin restoration, hierarchical clustering was performed based on relative protein abundance across the five time points (Figure 1F). Using the Nascent time point as the starting point of chromatin restoration (the first 15 min), and late G1 phase as the endpoint (14 h), clusters were grouped into four categories: clusters showing a 1.2-fold or more enrichment between the Nascent time point and any other time point were named "Enriched in nascent." Clusters showing a 1.2-fold or more enrichment between G2/M and any other time point were named "Enriched in G2/M." Clusters showing a 1.2 to 0.83-fold enrichment between Nascent and late G1 phase were named "Restored within 15 min," as they included proteins equally abundant 15 min after the passage of the fork and 14 h later. Finally, clusters showing a 0.83-fold or less enrichment between Nascent and late G1 time points were named "Delayed restoration."

Within the first 15 min after the passage of the replisome, 47.9% of the proteins identified were restored onto newly replicated DNA, while 25.1% were delayed (Figure 1G, 15 min). Delayed proteins bind onto chromatin following distinct kinetics, as shown in clusters 12, 9, 3, and 18 (Figure 1F). Interestingly, when cells reached mitosis, 14.9% of the identified proteins had not completed their restoration yet (Figures 1G and 5H). The most delayed proteins included proteins such as Histone H1, H2A-Z, and several TFs (Table S1). Similar results were obtained when only the major constituents of chromatin are selected using intensity-Based Absolute Quantification (iBAQ) values (Figures S1G and S1H). Clustering analyses therefore indicate that although most chromatin

Figure 1. Proteomic profiling of replicated chromatin from S phase to the subsequent G1 phase

(A) DNA replication provokes chromatin disassembly. New and old histones (darker and lighter pink) are incorporated onto newly replicated DNA. How other chromatin components reassembled is unknown.

(B) NCC-TMT time course analysis in HeLa S3 cells. Cell cycle progression monitored by flow cytometry. One representative experiment of six is shown.

(C) Heatmap of the relative abundance for identified replisome components, indicated as the average of percentage of enrichment (n = 6). Each column represents a time point (Nasc, LateS, G2/M, early G1, late G1), each row corresponds to the protein indicated on the left. The sum of each row corresponds to 100% of enrichment. The scale is indicated and common to the whole figure.

(D and E) Heatmaps showing MCM helicase complex and mitotic proteins (D) and examples of delayed proteins (E).

(F) Heatmap of hierarchical clustering into 18 clusters of 1,450 proteins (rows) along the cell cycle (columns) based on percentage of enrichment. Each cluster number is indicated on the left and in Table S1. Clusters were grouped according to their trend in four groups: Enriched in nascent (purple), Enriched in G2/M (blue), Restored within 15 min (green), and Delayed (orange). Right, the averages of protein enrichments of each cluster (thin lines) and average per group (thicker lines). Standard deviation is shown.

(G) Percentage of proteins belonging to indicated groups. In nascent chromatin, percentages correspond to the cluster groups from (F). In other timepoints, delayed proteins that are recruited onto chromatin switch from "Not restored yet" (orange) to "Restored proteins" (green) until they reach the pre-replication state (all chromatin is restored). See also Figure S1 and Table S1.

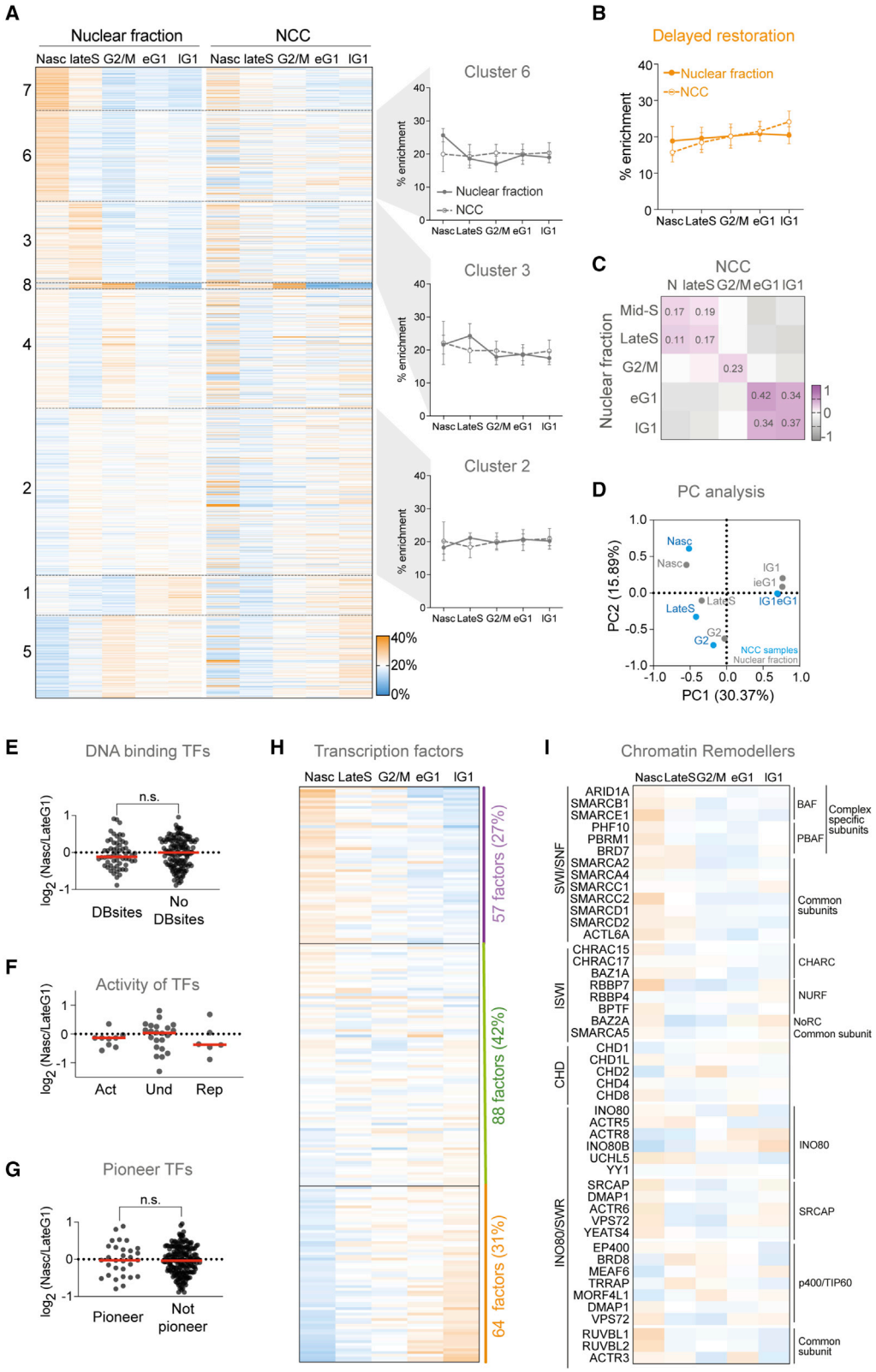

(legend on next page)

components are restored within the first 15 min after the passage of the replisome, for 212 proteins chromatin restoration is completed after mitosis, in daughter cells. Gene ontology (GO) term enrichment analysis of "Enriched in nascent" and "Enriched in G2/M" proteins included, as expected, proteins linked to "DNA replication" and "mitotic cytokinesis," respectively (Figure S1I). The "Delayed restoration" and "Restored within 15 min" categories, on the other hand, shared many GO terms such as "chromatin binding" and "histone modification," suggesting that GO term analysis alone will not suffice to understand how proteins regain access to replicated DNA.

Reassociation timing is independent of nuclear abundance

The finding that the reassociation of many related proteins occurs with distinct kinetics raises the question of what determines the rate at which proteins reassociate with chromatin. First, we tested whether most abundant proteins would be the first to reassociate to replicated DNA by mass action. However, using iBAQ values as a proxy for absolute abundance, the first proteins to bind newly replicated DNA were not more abundant than delayed proteins (Figure S2A). Previous work has shown that only 15% of the variance in chromatin signal can be explained by coinciding changes in cellular protein abundance.[22] To test if this was true for changes in nuclear abundance and chromatin restoration, nuclei were isolated by mechanical fractionation and nuclear fractions analyzed by TMT quantitative mass spectrometry in parallel with each NCC sample (Figure S2B and Table S2). As a control for cell cycle progression, proteins with known cell cycle-dependent variation in cellular abundance[22] were monitored (Figure S2C). Hierarchical clustering was performed based on nuclear abundance and aligned with replicated chromatin abundance (Figure 2A). In general, changes in nuclear abundance of a protein were not predictive of its recruitment dynamics to replicated DNA. This was also true for the "Delayed restoration" and "Restored within 15 min" categories defined in Figure 1F (Figures 2B and S2D). Consistent with this, the composition of nuclear and replicated chromatin fractions were compared using Pearson's correlations (Figure 2C) and principal-component analysis (PCA) (Figure 2D) and showed limited positive correlation (r = 0.17–0.42). Of note, the correlation distribution was not random and showed a certain degree of dependency on cell cycle phases. Overall, changes in nuclear abundance were not predicative of their timing of association to replicated DNA. Therefore, increasing the production of a protein is not a general strategy to ensure its rapid reassociation to replicated DNA.

Newly replicated chromatin contains an excess of selected TFs and chromatin remodelers

Another possible explanation for differential recruitment is that in nascent chromatin, histones are hyperacetylated and DNA is exposed.[9] However, proteins containing a bromodomain, a DNA binding domain, or exhibiting a net positive charge, do not bind more rapidly to newly replicated DNA (Figures S2E–S2G). Similarly, TFs containing a DNA binding domain[23] do not bind more rapidly to new DNA (Figure 2E). There was also no differential recruitment between TFs involved in transcriptional activation or repression (Figure 2F),[24] between those sensitive to DNA methylation or not[25] (Figure S2H), or factors acting as mitotic bookmarkers[26] (Figure S2I). Moreover, from the TFs defined as pioneer TFs (able to bind nucleosomal DNA),[27] only half regained immediate access to new DNA (Figures 2G and S2J). Altogether, these data revealed that the ability of proteins, including TFs, to gain access to newly replicated DNA cannot be inferred from known determinants. Interestingly, of the 209 TFs identified in at least four out of six experiments, 57 were enriched on nascent chromatin to levels beyond those observed at any other time point (Figure 2H). This was surprising, as chromatin accessibility over TF binding sites is globally lost on newly replicated DNA.[7,8] Of note, the transient enrichment of TFs on newly replicated chromatin was also observed when selecting the most abundant TFs (Figure S2K), revealing that access to newly replicated chromatin is not determined by the abundance of a TF on chromatin. Finally, the majority of ATP dependant chromatin remodelers were also enriched onto nascent chromatin (Figure 2I), revealing that newly replicated chromatin contains an excess of selected TFs and chromatin remodelers.

Chromatin restoration dynamic is conserved in human TIG-3 cells

To test the general applicability of the findings above in HeLa S3 cells using NCC, we next monitored chromatin restoration in a

Figure 2. Nuclear abundance and physico-chemical properties of a protein are not predicative of its reassociation timing

(A) Hierarchical clustering of percentages of enrichment from the nuclear fraction using the same strategy as in Figure 1F. The relative enrichments calculated for NCC samples were aligned to the clustered nuclear fraction. Only common identified factors are clustered (1,454 proteins, n = 3). Color scale is indicated and used throughout Figure 2. Right, average of enrichment of the nuclear fraction (straight line) and NCC (dotted line) for three indicated clusters. Standard deviations are shown.

(B) Average percentage of enrichment of NCC samples (dotted line) and nuclear fraction (straight line) of delayed proteins from Figure 1F. Standard deviations are shown (n = 3).

(C) Pearson correlation map of NCC and nuclear fraction datasets.

(D) Principal-component analysis of NCC (blue) and nuclear fractions (gray).

(E) Log_2 ratios of nascent chromatin and late G1 abundance of the TFs classified in two groups, harboring a DNA binding site or not. Red line, median; p value calculated using an unpaired t test.

(F) Same as in (E) for TFs classified as activators, repressors, or undetermined.

(G) Same as in (E) and (F) for identified pioneer TFs.

(H) Heatmap showing identified TFs in at least four out of six experiments, classified with the criteria defined in Figure 1F. Number of TFs per group and the percentage they represent are indicated on the right.

(I) Relative enrichments of chromatin remodelers (identified in at least four out of six experiments) classified by families (SWI/SNF, ISWI, CHD, or INO80). See also Figures S1 and S2, Tables S1 and S2.

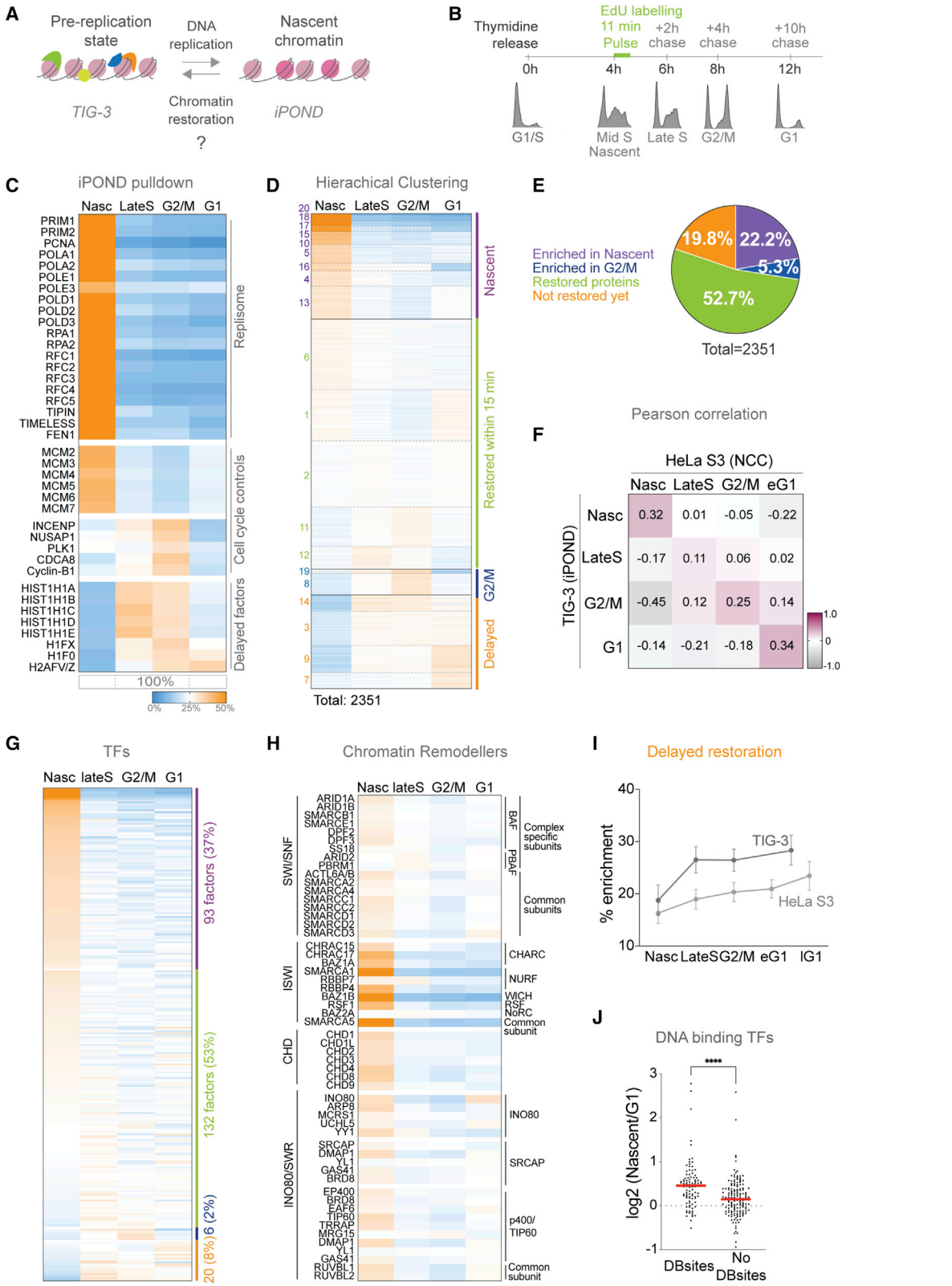

(legend on next page)

non-cancerous human cell line (TIG-3) using iPOND, a different method to label newly replicated DNA[19] (Figure 3A). Unlike HeLa S3, TIG-3 cells are finite and P53 positive. Unlike NCC, iPOND relies on EdU labeling on newly replicated DNA followed by click-it chemistry to attach the biotin tag to EdU. In mid-S phase, newly replicated DNA was EdU labeled for 11 min, and cells collected up to 10 hours after the EdU labeling (Figure 3B). Replicated chromatin was TMT labeled and analyzed by mass spectrometry. Five independent biological replicates were performed (Figure S3A) and 2,351 proteins were identified in all time points in at least four out of five experiments (Table S3). Core replisome components, mitotic proteins, and known delayed proteins exhibited the expected patterns (Figure 3C), supporting that replicated chromatin has been successfully isolated by iPOND in cycling TIG-3 cells.

Similar to HeLa S3, in TIG-3 most proteins reassociate within minutes to newly replicated DNA while hundreds bind only after mitosis (Figures 3D and 3E). Abundance (Figures S3B–S3D), abundance changes (Figures S3E–S3G), and physicochemical properties (Figures S3H–S3N) of a protein were also not predicative of its reassociation timing. Moreover, although proteins vary between the two-cell lines (Figure 3F), newly replicated chromatin in TIG-3 cells also contained an excess of TFs and remodelers (Figures 3G and 3H). Three key differences were detectable between the two cell lines. First, although cell cycle length is longer in TIG-3 cells (30 h) compared with HeLa S3 (24 h), chromatin restoration was faster in TIG-3 cells, most proteins having regained access to chromatin within 2 h after the passage of the fork (Figure 3I). Second, in TIG-3 cells, TFs with DNA binding domain were more enriched on newly replicated chromatin than TFs without DNA binding domain (Figure 3J). Third, although all chromatin remodelers were enriched on newly replicated chromatin in both cell lines, the ISWI family was highly enriched in TIG-3 cells (Figure 3H), suggesting a more prominent role for ISWI behind replisomes compared with other remodeler families in this cellular context. The reasons for these three differences could be due to cellular context or the iPOND labeling being shorter than NCC labeling. In conclusion, the TIG-3 analysis supports that newly replicated chromatin contains transiently an excess of TFs and chromatin remodelers, that most chromatin components are restored within minutes after the passage of the replisome, and that full chromatin restoration is only completed until after mitosis.

Chromatin restoration is different between euchromatin and heterochromatin

We next compared chromatin restoration between euchromatin and heterochromatin to test whether chromatin organization affects protein access to replicated DNA (Figure 4A). Indeed, reduced accessibility to heterochromatin has been proposed to restrict protein access to DNA.[28–30] Active and open euchromatic regions are replicated in early S phase, and repressed heterochromatic regions are replicated in late S phase.[31] Therefore, we took advantage of this replication timing difference to biotin-dUTP label euchromatin and heterochromatin and compared chromatin restoration in these two regions. HeLa S3 cells were synchronized at the G1/S phase border, released in S phase, and DNA was biotin-dUTP labeled 2 h (early S phase) or 5.5 h after release (late S phase) (Figure S4A). Replicated chromatin was isolated immediately behind the fork (Nasc), in G2/M phase (G2/M), early G1 phase (eG1), and late G1 phase (lG1) (Figure 4B). NCC was coupled to TMT labeling. Three independent biological replicates were performed (Figure S4B) and 2,581 proteins were detected in all conditions (Table S4). To confirm that early and late replicated regions were isolated, we performed Repli-seq using our synchronization strategy (Figure 4C) and compared the genomic regions recovered with replication timing data available for HeLa S3 cells (Figure 4D) (ENCODE Project Consortium, 2012).

In early and late replicated regions, replisomes and mitotic factors peaked in Nascent and G2/M, respectively (Figure 4E). However, two distinct chromatin regions were isolated. Early replicated regions contain higher levels of RNA Polymerase II and Topoisomerase 1, that alleviates torsional stress during transcription, while late replicated regions were more abundant in lamins and nucleopore components, consistent with their localization to the nuclear periphery[31] (Figure 4E). Of note, both lamina and nucleopore components drop in abundance transiently in late replicated regions in early G1 phase as cells exit mitosis, reflecting chromatin transient loss of attachment to the nuclear membrane at this time.[32] GO term analysis confirmed that most enriched factors in early replicated regions were

Figure 3. Chromatin restoration dynamic is conserved in human TIG-3 cells

(A) Same as Figure 1A, using TIG-3 cells and iPOND.

(B) Experimental design of the iPOND-TMT time course analysis in TIG-3 cells (n = 5). Cell cycle progression monitored by flow cytometry. One representative experiment of five is shown.

(C) Heatmap of relative abundance of identified replisome components, MCM helicase complex, five mitotic factors, and examples of delayed proteins shown as the average of the percentage of enrichment (n = 5). Each column represents a time point (N, LateS, G2/M, and G1) and each row corresponds to the protein indicated on the left. The sum of each row corresponds to 100% of enrichment. Color scale indicated and used throughout Figure 3.

(D) Hierarchical clustering into 20 clusters (2,351 proteins, n = 5). Cluster number is indicated on the left and in Table S3. Clusters are grouped in four groups: Enriched in nascent (purple), Restored within 15 min (green), Enriched in G2/M (blue), and Delayed (orange).

(E) Groups identified based on (D) hierarchical clustering. The percentage of proteins for each group is shown.

(F) Pearson correlation between HeLa S3 and TIG-3 cells.

(G) Identified TFs classified by the clusters they belong to from (D).

(H) Identified chromatin remodelers classified by family (SWI/SNF, ISWI, CHD, INO80/SWR).

(I) Average of enrichments for Delayed proteins in HeLa S3 (NCC, Figure 1F) and TIG-3 (iPOND, Figure 3D). Standard deviations are shown.

(J) Log_2 ratios of the nascent chromatin and late G1 abundance of TFs harboring a DNA binding site or not. Red line, median; p value calculated using an unpaired t test. See also Figure S3 and Table S3.

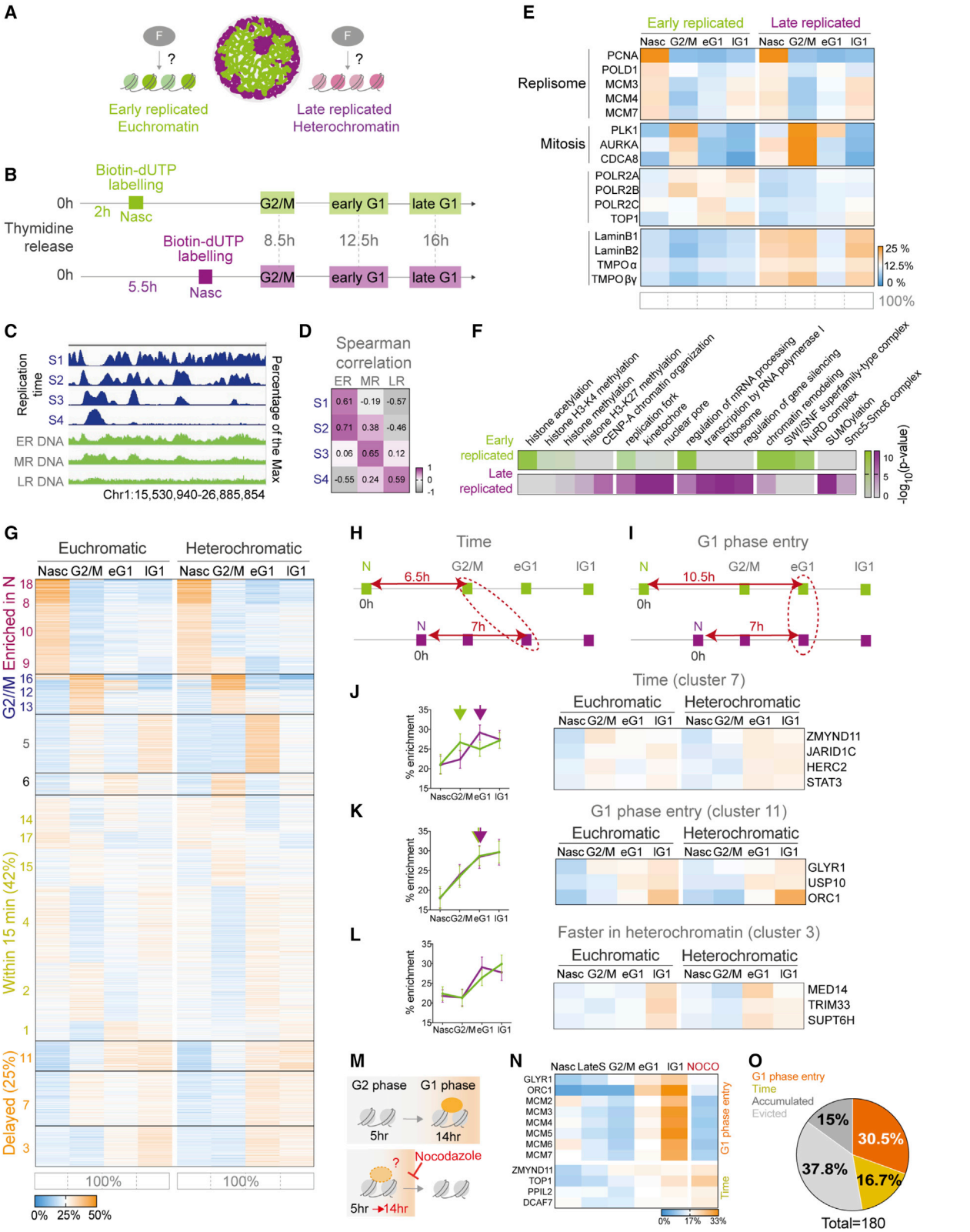

(legend on next page)

associated with euchromatic features such as histone acetylation, transcription, and remodeling, while the most enriched factors in late replicated regions were linked to heterochromatin features such as gene silencing (Figure 4F). Altogether, these observations supported the successful isolation of two distinct chromatin regions from the moment of their assembly and throughout subsequent G2 and G1 phases.

Next, we performed hierarchical clustering (Figure 4G). To ensure that the clustering was not prejudiced by the global differences in abundance of the proteins between euchromatic and heterochromatic regions, the sum of intensities for euchromatic and heterochromatic regions were normalized. Hierarchical clustering performed without this normalization step is shown in Figure S4C and did not modify clustering results. Forty-two percent of the identified proteins re-associated within the first 15 min to newly replicated DNA in both euchromatin and heterochromatin (Figure 4G) and were in good accordance with the mid-S phase dataset (Figure S4D). Twenty-five percent did not reassociate within 15 min and restoration kinetics were different between euchromatin and heterochromatin for two clusters (11 and 3) out of three. Therefore, within the first 15 min, chromatin organization does not affect the ability of a protein to bind replicated DNA. However, for proteins that do not bind within the first 15 min, chromatin organization can affect their ability to bind newly replicated DNA.

Other notable differences were two clusters of proteins peaking at different cell cycle phase (Figure 4G, Clusters 5 and 6). Cluster 5 peaks in G2/M and late G1 phase in euchromatin while peaking in early G1 phase in heterochromatin. This cluster included a large proportion of recombinant DNA associated proteins and ribosomal proteins (Figure S4E) and were enriched in heterochromatin (Figure S4C). Cluster 6 on the other hand peaks in G2/M phase in heterochromatin while remaining relatively even in euchromatin. Further inspection of this group revealed chromatin factors such as HP1 and ESCO1 (See Figure 5).

G1 phase entry is required for full completion of chromatin restoration

Clustering revealed that delayed proteins were distributed into three clusters. In cluster 7, proteins reassociate in G2/M in euchromatin and in early G1 phase in heterochromatin (Figure 4H, dashed ovals). Despite this apparent difference in reassociation speed, given that euchromatin was replicated 3.5 h before heterochromatin, proteins from this cluster took a similar amount of time since the passage of the fork to reassociate to replicated DNA. This cluster included proteins such as the histone demethylase JARID1C, the E3 ubiquitin ligase HERC2, the tumor suppressor ZMYND11, or the transcription activator STAT3 (Figure 4J). In cluster 11 on the other hand, the abundance of delayed proteins is similar in euchromatin and heterochromatin in early G1 phase (Figure 4I, dashed ovals). Therefore, it took 10.5 h to reassociate in euchromatin and only 7 h in heterochromatin, suggesting that G1 phase entry is required for its restoration. ORC1, USP10, and the KDM1B cofactor GLYR1 (Figure 4K) belong to this cluster. ORC1 was a good control within this cluster, as it binds both euchromatin and heterochromatin in G1 phase.[21]

The experiment above supports that, similar to CENP-A,[11] several proteins require G1 phase entry to fully reassociate to replicated chromatin. To directly test this prediction, we compared protein level in cells allowed to enter in G1 phase and cells blocked in G2/M, in both cases 14 h after the passage of the fork (Figures 4M, S4F, and S4G). Analysis confirmed that in

Figure 4. Chromatin environment and G1 phase entry influence the full completion of chromatin restoration

(A) Recruitment of a factor in compartment A and B.

(B) Experimental design.

(C) Repli-seq samples comparing early, mid and late replicated regions from this study with published Repli-seq samples of four S-phase fractions (S1, S2, S3, S4) (ENCODE Project Consortium, 2012) (n = 1).

(D) Spearman correlation of Repli-seq samples from (C).

(E) Average of the relative abundance of the indicated proteins across the eight samples (n = 3). Columns correspond to timepoints shown in (B) for early and late replicated labeled regions. Shown proteins are divided into four groups: replisome components, mitotic proteins, RNA pol II subunits, and lamins. Scale is indicated on the right.

(F) $-\log_{10}$ p values heatmap of the differentially found GO terms in early and late replicated labeled samples. Identified proteins were classified in two groups according to their enrichment in early or late replicated regions. The sum of intensities from four timepoints was considered.

(G) Hierarchical clustering in 18 clusters of 2,581 proteins (rows) along the cell cycle (columns) based on the percentage of enrichment per region (see bottom of the heatmap). Each cluster number is indicated on the left and in Table S4. Clusters were grouped according to their restoration trend in four groups: Enriched in nascent (pink), Enriched in G2/M (blue), Restored within 15 min (yellow), and Delayed (orange). Scale is at the bottom and common to (J), (K), and (L).

(H) Samples collected after the same time elapsed since the passage of the fork.

(I) Samples collected at the same cell cycle phase, regardless of the time elapsed since the passage of the fork.

(J) Enrichment of proteins that need a certain period of time after DNA replication to be recruited to chromatin (cluster 7 from G). Protein levels in euchromatin (green line) and heterochromatin (purple line) are shown. Arrows represent the moment when proteins reach their complete restoration. Right, some examples are shown.

(K and L) Same as in (J) for proteins dependent on the entry in G1 phase (cluster 11 from G) and proteins more rapidly recruited in heterochromatin (cluster 3 from G).

(M) Delayed protein restoration can be dependent on G1 phase entry or post-replication time. Nocodazole allows uncoupling of cell cycle progression from time and therefore deciphering of which ones regulate reassociation of delayed proteins.

(N) Examples of protein restoration dependent on G1 phase entry or post-replication time (n = 3).

(O) Classification of identified delayed factors depending on their behavior upon nocodazole treatment. Experiment was performed as in Figure 1B plus an additional sample treated with nocodazole for 12 h (see Figure S4 and Table S5, n = 3). Only proteins increasing from G2/M to late G1 were taken into consideration. See also Figure S4, Tables S4 and S5.

addition to MCMs,[33] several delayed factors such as GLYR1 rely on G1 phase entry to bind replicated chromatin (Figures 4N and 4O and Table S5). In contrast, factors such as ZMYND11 bind to chromatin in G2/M arrested cells, revealing that their restoration does not rely on G1 phase entry, and requires time instead to associate to replicated chromatin. Of note, many proteins have accumulated or were evicted upon nocodazole arrest as expected from arresting cells using cell cycle inhibitor (Figure 4O).[34] Altogether, this analysis confirms that G1 phase entry is a requirement for the assembly of a subset of delayed proteins, and that chromatin restoration can therefore not be completed prior to mitosis.

Restoration of heterochromatin is faster than euchromatin

In cluster 3, proteins exhibited a more rapid restoration in heterochromatin compared with euchromatin (Figure 4L). This cluster included proteins such as the histone chaperone SUPT6H, the mediator of RNA polymerase II MED14, and the E3 ubiquitin ligase TRIM33. This cluster also included several core heterochromatin factors as defined by biophysical methods coupled to proteomics.[28] None of these factors were exclusively present in heterochromatin, but they regained a faster access to heterochromatin compared with euchromatin (Figure S4H). Because H3K27me3 is more rapidly re-established in H3K27me3-rich regions,[35] one possibility is that histone modification re-establishment contributes to heterochromatin restoration speed. To test this possibility, we monitored the restoration of heterochromatin in the presence of an EZH2 inhibitor, which blocks H3K27me3 re-establishment (Figures S4I and S4J). Blocking H3K27me3 restoration reduced the assembly of the Polycomb complexes (Figure S4K) and of an additional 156 non-Polycomb-delayed proteins such as Histone H1 and DNMT3A (Figure S4L and Table S6). Therefore, the re-establishment of H3K27me3 behind replisome contributes to heterochromatin reassembly. Moreover, it is known that H3K27me3 stimulates PRC2 activity and is recognized by PRC1, playing a central role in maintenance of Polycomb chromatin domains.[36] These data support that this feedback mechanism is important for the maintenance of Polycomb chromatin domains following DNA replication.

The composition of euchromatic and heterochromatic regions is the most similar behind replisomes and the most different after mitosis

Our finding that most proteins reassociate within 15 min to newly replicated DNA in euchromatin and heterochromatin, led us to test the hypothesis that behind replisomes, these regions share many similarities. To this end, the composition of replicated euchromatic and heterochromatic regions was compared using Pearson's correlations (Figure 5A) and PCA (Figure 5B). Euchromatic and heterochromatic regions exhibited the strongest correlation in nascent chromatin ($r = 0.7$). This was also true when comparing early or late replicated regions with mid-replicated regions (Figures S5A and S5B). Therefore, DNA replication increases the similarities between euchromatin and heterochromatin. Interestingly, the correlation between euchromatic and heterochromatic regions decreased along the cell cycle but not in a linear way. In early G1 phase euchromatin and heterochromatin exhibited the poorest correlation ($r = -0.4$) (Figure 5A). These differences were not due to a loss of cell cycle synchronization, as in early G1 phase nuclear fractions correlation Vremained strong (Figure 5C), and G1 phase cell cycle regulators were expressed as expected (Figure S5C). Therefore, DNA replication tends to reduce transiently the differences between euchromatin and heterochromatin, while mitosis enhances them, suggesting that while DNA replication alters the chromatin template,[8] mitosis may reinforce their specificity.

Reorganization of interphase chromatin as cells progress through mitosis

Many proteins show distinct timing of association, distinct abundance, or both, between euchromatin and heterochromatin. One of the most dissimilar groups of proteins in early G1 phase were the Structural Maintenance of Chromosome (SMC) protein families and their regulators (Figures 5D and 5E). In contrast, and consistent with the loss of attachment of heterochromatin from the nuclear membrane in early G1 phase, nuclear pore components and lamins were similar in euchromatin and heterochromatin at this time point (Figures 5F and 5G).

In euchromatin, condensin I and II peaked in G2/M phase, in accordance with their role in chromosome compaction (Figure 5H). In heterochromatin, condensin I and II peaked in early G1 phase. This difference was not due to a loss of cell cycle synchronization (Figures 5C and 5I), nor to a delay in DNA decatenation upon chromosome compaction as TOP2A and TOP2B were peaking in G2/M in both regions (Figure 5J). This raises the question of how mitotic chromosome condensation is achieved in heterochromatin where association of condensin is delayed. An intriguing possibility is that additional factors contribute to mitotic condensation. Candidates include proteins within cluster 6 (Figure 4G) that associate earlier with heterochromatic regions during mitosis, such as HP1 complex (Figure 5K) and the SMC5/6 proteins (Figure 5L), which have recently been linked to chromatin compaction.[37]

Cohesin rings (SMC3, SMC2, and SCC1) were enriched in S phase and equally abundant on euchromatin and heterochromatin (Figure 5M). However, Sororin, which prevents sister chromatids cohesion removal, was more abundant in heterochromatin and retained in G2/M, consistent with sister chromatids cohesion retention at centromeres.[38] Cohesin rings, that promote loop extrusion in interphase,[39] its regulatory factors (ESCO1, MAU2, NIPBL, WAPAL), and the loop stabilizer CTCF, were more abundant in euchromatin. This was surprising given that CTCF binding sites are evenly distributed along the genome,[40] but is consistent with the loop extrusion function in transcription.[41] Altogether, this analysis reveals differences in abundance of SMC rings and their regulatory factors and raises the possibility that assembling and disassembling mitotic chromosomes may be overcome by distinct strategies in euchromatin and heterochromatin.

Identification of proteins involved in euchromatin and heterochromatin assembly

Next, we inspected proteins involved in DNA replication and chromatin assembly to identify proteins with potential specific

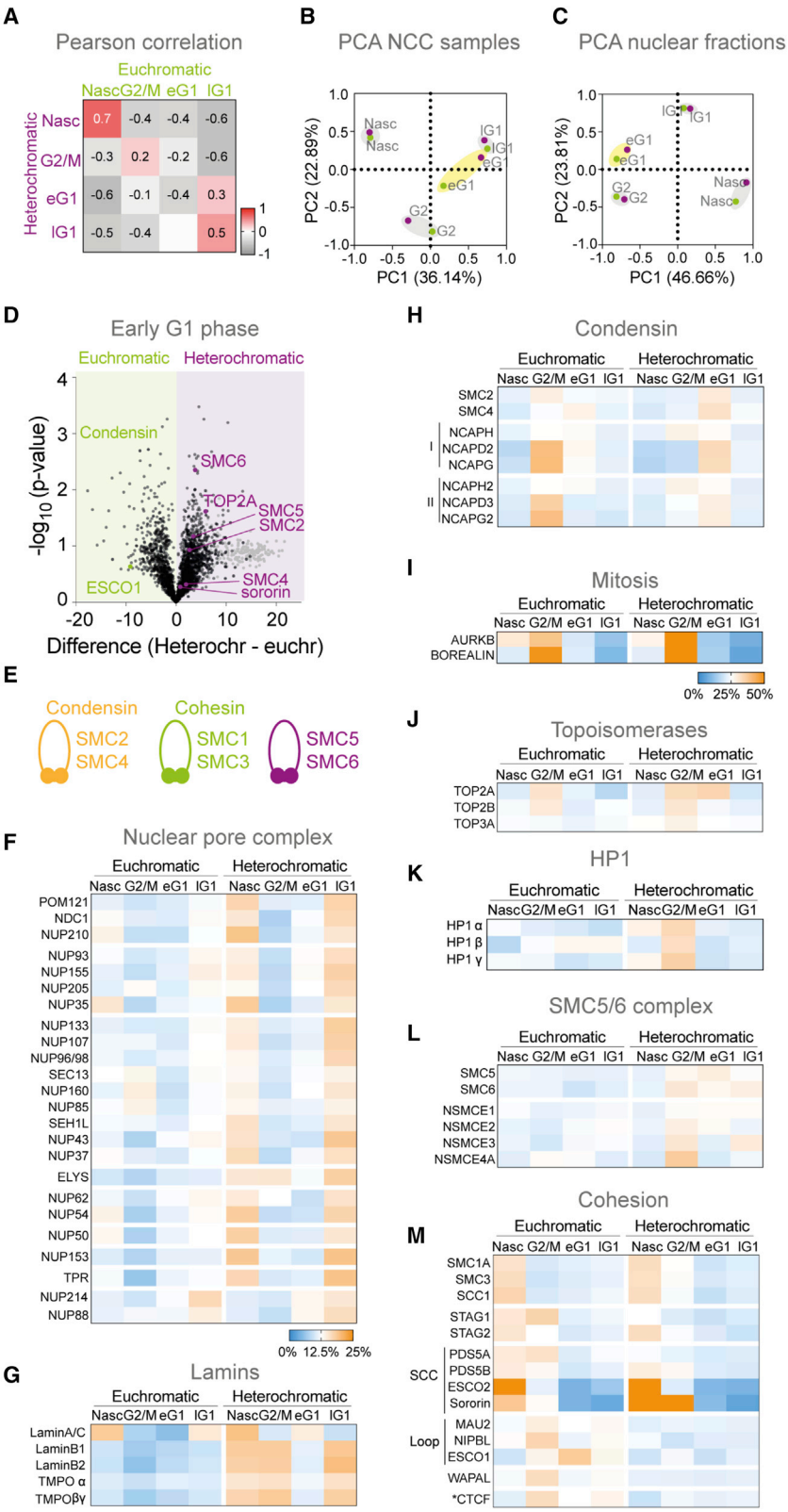

Figure 5. Reorganization of interphase chromatin as cells progress through mitosis

(A) Pearson correlation comparing euchromatin and heterochromatin using percentage of enrichment relative to eight samples.

(B) Principal-component analysis of euchromatin (green dots) and heterochromatin (purple dots) NCC samples.

(C) Equivalent to (B) for nuclear fraction samples.

(D) Volcano plot comparing protein abundance in euchromatin and heterochromatin in early G1 phase showing proteins of interest (n = 3).

(E) Main components of the three SMCs subfamilies.

(F–M) Percentage of enrichment heatmaps of indicated group of proteins (average is shown, n = 3). Percentages of enrichment are calculated according to eight samples, except (I) where percentages are calculated per region (four samples). SCC, sister chromatid cohesion.Scales shown. See also Figure S5 and Table S4.

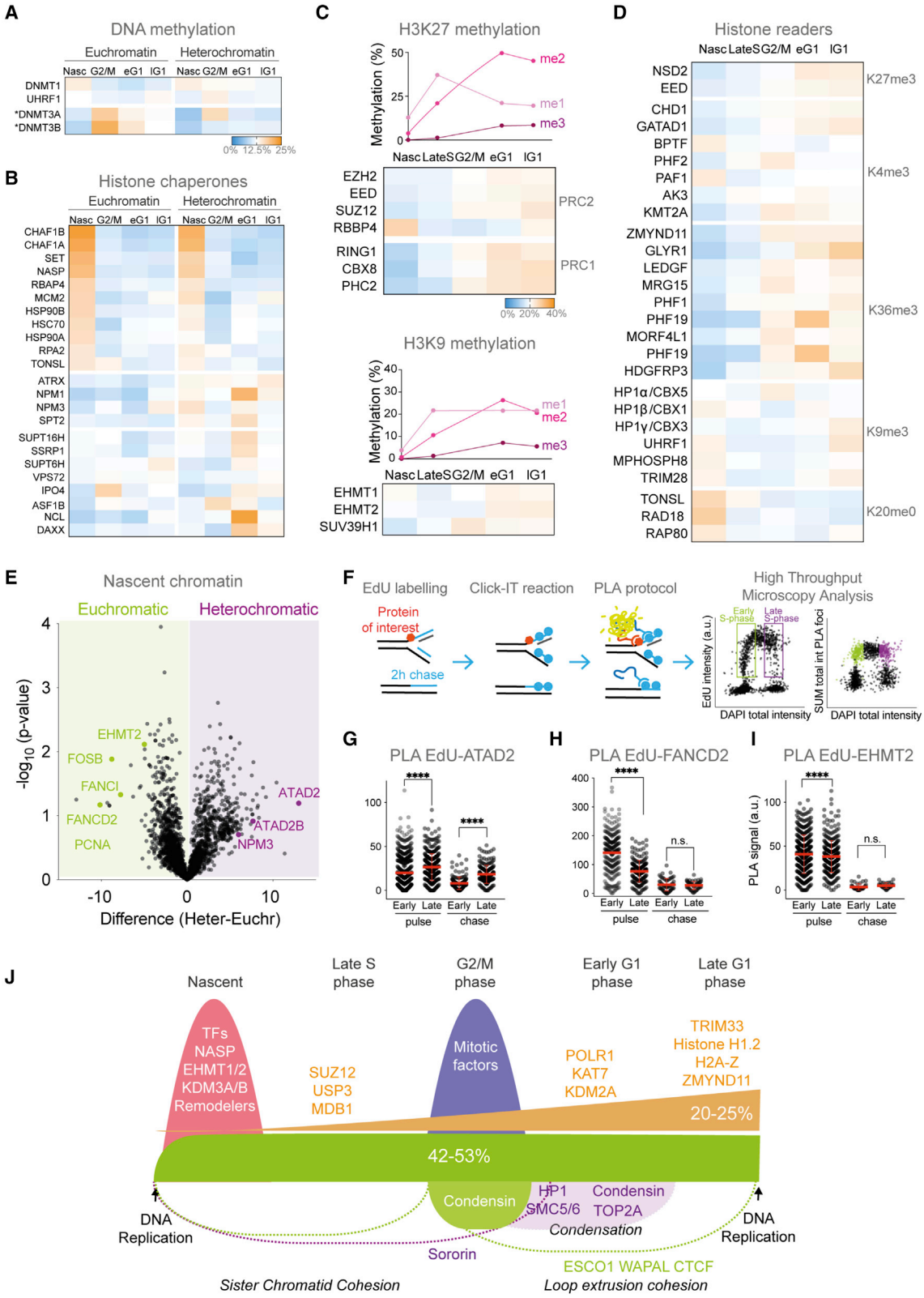

(legend on next page)

function within euchromatin or heterochromatin. Replisome core components were equally abundant on nascent euchromatin and heterochromatin (Figure S6A). DNMT1 was also equally abundant, consistent with its DNA replication coupled DNA methylation function[42] (Figure 6A). On the other hand, DNMT3A and B were peaking in G2/M and were less abundant in heterochromatic regions and may be the cause of the global hypomethylation of late replicated regions in cycling cells.[43]

The histone chaperones CAF-1 p150, p60 and p48, MCM2, and RPA2 were equally abundant on newly replicated euchromatic and heterochromatic regions, consistent with their replication coupled chromatin assembly functions[44] (Figure 6B). However, NPM3, NPM1, SPT2, and ATRX were enriched in heterochromatin. In the case of NPM1, this is consistent with its recently discovered function in handling parental histones within Polycomb target regions, replicated in late S phase in HeLa S3 (ENCODE Project Consortium, 2012),[45] and for ATRX, with its function in H3.3 assembly within heterochromatin.[46] A general role for NASP in replication coupled chromatin assembly and for SPT2 and NPM3 in heterochromatin remain to be tested. Interestingly, none of the histone chaperones identified were enriched in euchromatin compared with heterochromatin, suggesting that at the fork, within euchromatin, histones are not handled by specialized histone chaperones.

Histone writers' recruitment mirrors the establishment of their cognate modifications

Once incorporated, newly synthesized histones must be methylated to ensure the propagation of histone methylation patterns. It remains unclear which histone modifier oversees this process (Figure S6B). Histone methylation kinetics have been described for regions replicated in mid-S phase in HeLa S3 cells,[10] thus, we compared histone methylation establishment kinetic with the recruitment of their cognate methyltransferases (KMTs) and demethylases (KDMs) identified in the mid-S phase dataset (Table S1). Overall, the presence of KMTs mirrors the establishment of their cognate modifications. For instance, H3K27me3 and EZH2 levels (together with the rest of the Polycomb complex 2 and 1) are low abundant on newly replicated chromatin and subsequently gradually increase along the cell cycle (Figure 6C). Similarly, H4K20me2/SUV4-H2 levels mirror each other's (Figure S6C). For H3K9, we detected a sequential recruitment of EHMT1/2 imposing me1-2, followed by SUV39H2 imposing me3 (Figure 6C). Moreover, in general, KDMs also mirror the abundance of their target modifications and the presence of the corresponding KMTs (Figure S6D), supporting that the establishment of methylation on newly synthesized histones is the result of concomitant methylation/demethylation events. Finally, when comparing euchromatin and heterochromatin, the abundance of histone modification correlates with the abundance of their cognate KMTs and KDMs (Figure S6E). For instance, H3K4me3 KMT and KDM were more abundant in euchromatic regions, where H3K4me3 is more abundant. The two exceptions were KDM5A and KDM5C, two H3K4me3 KDMs, detected within heterochromatic regions in G1 phase. This could reflect a counteracting measure to spurious transcription.[47]

Histone readers were not diluted by two on newly replicated chromatin like their cognate modification but exhibited a milder dilution of 1.45 instead (Figure 6D). This suggests that most histone readers have other means to bind newly replicated chromatin. The exceptions to this rule were H4K20me0 readers, which is a hallmark of newly synthesized histones.[48] The second exception was H3K9me3 readers. This may be due to the known coupling between CAF-1 at replication fork and H3K9me3 readers HP1 and TRIM28.[49] Consequently, H3K9me3-associated silencing may be stably maintained behind replisomes despite the drop of H3K9me3 itself while H3K27me3-associated silencing may be challenged. Therefore, although H3K9me3 and H3K27me3 rely on a reader-writer mechanism to propagate,[50] H3K9me3 itself may be less essential for its propagation than H3K27me3. Finally, several HATs, HDAC, and E3 ligases were also identified (Figures S6F and S6G). Most notable enrichment on newly replicated chromatin were HAT1 and HDAC1, which have been previously linked to handling newly synthesized histones at the fork.[51,52] The E3 ligase HUWE1 and ANAPC1 on the other hand have not been previously directly linked to DNA replication.

Figure 6. Identification of proteins involved in euchromatin and heterochromatin restoration

(A) Identified DNA methyltransferases and UHRF1. Scale is shown, enrichment calculated according to eight samples (average, n = 3).

(B) Histone chaperones classified in three groups: enriched in nascent chromatin in both regions, only in heterochromatin, not enriched in nascent chromatin. Same scale as (A).

(C) Top, percentages of methylation for indicated histone modification in Nasc, Late S, G2, and G1 phase from Alabert et al.[10] Bottom, identified writers and/or readers specific of the indicated histone modification in mid-S replicated regions mass spec dataset (Table S1). Scale is shown and common to (D).

(D) Histone readers of H3K27, H3K4, H3K36, H3K9, and H4K20.

(E) Volcano plot comparing protein abundances in nascent euchromatin and heterochromatin highlighting relevant proteins (n = 3).

(F) PLA analysis by HTM of EdU and protein of interest: HeLa S3 cells were EdU labeled, nascent chromatin and 2 h chase samples were collected. Click-IT and PLA protocols were performed, and images acquired and analyzed detecting DAPI, EdU, and PLA intensities. Early and Late replicating cells were gated as shown, and the SUM of the total intensity of the PLA foci from these regions was calculated.

(G–I) Single-cell PLA signal of EdU-ATAD2, EdU-FANCD2, and EdU-EHMT2 interaction, respectively. They are classified in early and late replicated regions and nascent chromatin (pulse) and 2 h mature chromatin (chase). PLA signal was calculated as the SUM of the total intensity of PLA foci per nucleus and normalized according to EdU intensity per cell. Red line, average; Standard deviation is shown. Unpaired and two-sided t test was used. One representative experiment is shown (n = 3, three technical replicates each, >30 cells measured per technical replicate, >150 cells per biological replicate).

(J) Most proteins regain access within the first 15 min after replisomes (green). 20% to 25% of the identified proteins do not (orange). Replisome components, TFs, chromatin remodelers and several histone KDMs and KMTs are enriched in nascent chromatin (red). Bottom, the SMC kinetics are shown as dashed lines in euchromatin (green) and heterochromatin (purple). See also Figure S6 and Tables S1 and S4.

Preferences toward euchromatin or heterochromatin are dynamic

The only complete DNA repair pathway with a preference toward euchromatin or heterochromatin was the MissMatch Repair pathway (Figure S6H, a complete list of DNA repair components as defined in Olivieri et al.[53] is available in Table S7). This finding directly supports the hypothesis that recruitment of different DNA repair pathways and not different level of lesions is the primary cause of the higher point mutation rate observed in late replicated regions.[54] FANCD2 and its binding partner FANCI were also enriched in euchromatin (Figure 6E). As the rest of the Fanconi anemia pathway was equally abundant on euchromatin and heterochromatin (Table S7), it supported the Fanconi anemia independent role for FANCI/D2 in euchromatin.[55]

Finally, we identified several proteins with unexpected enrichment in euchromatin or heterochromatin. We selected two factors, FANCD2 and ATAD2, and used quantitative image-based cytometry (QIBC) combined with Proximity Ligation Assay (PLA) as an orthogonal approach to validate the differential enrichment between newly replicated euchromatic and heterochromatic regions (Figure 6F). First, we confirmed FANCD2 and ATAD2 transient enrichment on nascent chromatin (Pulse versus Chase), and second, their preference toward euchromatic or heterochromatic regions (Pulse Early versus Pulse Late) (Figures 6G and 6H). EHMT2 was used as a positive control for protein biased toward euchromatic regions[56] (Figure 6I). Interestingly, FANCD2 enrichment on euchromatic region was not due to transcription replication conflicts but disappeared in conditions of replicative stress (Figure S6I). Altogether, it revealed that these differential enrichments are not intrinsic to chromatin regions, and instead are responsive to the nuclear environment.

DISCUSSION

In summary, our study provides a detailed picture showing the kinetics of protein binding to newly replicated DNA over different regions of the genome (Figure 6J). We show that a generalized mechanism cannot explain most recruitment events, but each mechanism could explain a fraction. We identified three main kinetics of protein binding, "Restored within 15 min," "Delayed restoration," and "Enriched in Nascent," with several implications for our understanding of how chromatin-based information is transmitted through cell division.

Regaining access to newly replicated DNA

Most factors reassociate with chromatin to levels observed throughout the cell cycle within minutes (Figures 1 and 3). We show that their rate of assembly onto newly replicated DNA was independent of their function, physicochemical properties (Figures 2 and 3), and the regions they reassociate to, euchromatin or heterochromatin (Figure 4). During S phase, the abundance of these factors must be sufficient to ensure the supply required to load an additional copy of the genome. It is likely that this is achieved through an excess of these factors through most of the cell cycle, as we do not observe cell cycle-dependent changes in the nuclear abundance of these proteins (Figure 2). Interestingly, 42% of the TFs identified in HeLa S3 and 53% in TIG-3 cells regained immediate access to newly replicated DNA. It has been shown previously that many TFs are retained on mitotic chromosomes.[22,57] However, in mitosis, regulatory regions remain highly accessible[22] while chromatin accessibility over TF binding sites is globally lost on newly replicated DNA.[7,8] It is therefore possible that TFs bind regions that remain accessible on newly replicated chromatin. Alternatively, they may not associate initially to their target sites but re-localize upon transcription restart when nucleosomes regain their original position.[8]

Low abundance and loss of function

Twenty percent to 25% of the proteins identified show delayed reassembly onto newly replicated DNA, requiring more than 15 min to be restored to level similar to pre-replication (Figures 1G and 3E), which is consistent with histone modification studies.[10] Several of these factors are involved in transcriptional regulation, such as histone variants and histone modifiers. It is possible that the function they contribute to is on hold for the duration of their restoration, as in general the abundance of a protein reflects its function[58] and such disruption may occur at a subset of Polycomb regulated genes after DNA replication.[59] Alternatively, as shown for CENP-A,[11] their function may not be affected behind replisomes and the increase in abundance is required to cope with the subsequent dilution. Further work is needed to establish which chromatin-based processes are disrupted by DNA replication and for how long. This is an important question, as the disruption or dilution of pre-existing chromatin components during DNA replication were the initial mechanisms proposed to explain how, in certain conditions, transcriptional changes require DNA replication.[60,61]

Nascent chromatin, a land of opportunity or opportunists?

We found that many proteins were unexpectedly more strongly enriched on DNA within minutes of replication than at other stages in the cell cycle. These proteins include many TFs and remodeling enzymes (Figures 2 and 3). As this enrichment is observed in both cell lines analyzed and using two different technologies, it is possible that the nascent chromatin environment represents an opportunity for these factors to sample sites where stable occupancy does not normally persist through other stages in the cell cycle. There is a precedent for association of pluripotency TFs SOX2 and OCT4 at non-canonical sites in mitosis.[62] It is conceivable that in the presence of appropriate signals these transient interactions are stabilized. In this case, the transient overloading of these factors on newly replicated chromatin could represent a window of opportunity for establishing different expression programs.[3,63] Examples of transcriptional changes due to replication coupled incorporation of proteins on newly replicated DNA has been shown in DT40 cells upon replication stress[64] and suggested recently in mouse cells.[61] Our finding that DNA replication not only disrupts but also promotes recruitment of TFs provides a significant advance in understanding how DNA replication could contribute to programmed changes of cell memory. Future work using developmentally regulated cell systems will allow testing of the

hypothesis that TFs overloading to newly replicated DNA is a potential mechanism to promote transcriptional changes.

Limitations of the study

Using TMT-based relative abundance enables inspection of the changes of abundance for each individual protein across the different time points. Consequently, all proteins are treated equally, regardless of their absolute abundance in cells.

Only proteins identified in every time point of each experiment were taken into consideration in this analysis. Thus, a subset of proteins is not included in the study.

Analyzing replicated chromatin from synchronized and released cells leads to variability from experiment to experiment. Arresting cells with a cell cycle inhibitor, as shown for the nocodazole experiments, improves the reproducibility (Figure S1B) but may also reflect arrest-specific responses.[34]

STAR★METHODS

Detailed methods are provided in the online version of this paper and include the following:

- KEY RESOURCES TABLE
- RESOURCE AVAILABILITY
  - Lead contact
  - Materials availability
  - Data and code availability
- EXPERIMENTAL MODEL AND SUBJECT DETAILS
- METHOD DETAILS
  - Cell synchronisation
  - Drug treatments
  - Nascent chromatin capture
  - Isolation of proteins in nascent DNA (iPOND)
  - Immunoblotting
  - Flow cytometry
  - Microscopy
  - Mass spectrometry
  - Repli-seq protocol
- QUANTIFICATION AND STATISTICAL ANALYSIS
  - Mass spec data
  - High throughput microscopy data
  - FACS data
  - Sequencing data
  - Statistical analysis

SUPPLEMENTAL INFORMATION

Supplemental information can be found online at https://doi.org/10.1016/j.celrep.2023.111996.

ACKNOWLEDGMENTS

We thank Jane Wright, Tony Ly, and Giulia Saredi for critical reading of the manuscript, and Julian Blow lab for useful discussions. We thank the flow cytometry and imaging facilities in the School of Life Sciences. We also thank the ENCODE Consortium for the Repli-seq data. V.A. and E.G-W. were supported by the CRUK-CDF C57404/A21782. S.B. was supported by the ERC-Stg-IDRE. D.R.-S. was supported by an MRC-DTP PhD fellowship. H.J. was supported by Wellcome Collaborator Award (ref. 206293/Z/17/Z). J.H. was supported by Wellcome Trust Strategic Award (ref. 108058/Z/15/Z). E.G. was supported by a collaboration with DSTT and Boehringer-Ingelheim. Research in the Owen-Hughes lab is funded by MRC grant MR/SO21647/1. Research in the Alabert lab is funded by CRUK-CDF (C57404/A21782) and the European Research Council ERC-Stg-IDRE.

AUTHOR CONTRIBUTIONS

Conceptualization, V.A. and C.A.; methodology, V.A., C.A, S.B., H.J., J.H., and A.G.; validation, V.A., S.B., and D.R.-S.; formal analysis, V.A., S.B., H.J., D.R.-S., E.G.-W., J.H., N.W., and E.G.; investigation, V.A., S.B., H.J., D.R.-S., E.G.-W., J.H., N.W., and E.G.; writing – original draft, V.A. and C.A.; writing – review & editing, V.A., C.A., A.G., and T.O.H; funding acquisition, C.A.

DECLARATION OF INTERESTS

The authors declare no competing interests.

INCLUSION AND DIVERSITY

We support inclusive, diverse, and equitable conduct of research.

Received: June 5, 2022
Revised: August 12, 2022
Accepted: January 3, 2023

REFERENCES

1. Alabert, C., and Groth, A. (2012). Chromatin replication and epigenome maintenance. Nat. Rev. Mol. Cell Biol. *13*, 153–167. https://doi.org/10.1038/nrm3288.
2. Ramachandran, S., and Henikoff, S. (2015). Replicating nucleosomes. Sci. Adv. *1*, e1500587. https://doi.org/10.1126/sciadv.1500587.
3. Stewart-Morgan, K.R., Petryk, N., and Groth, A. (2020). Chromatin replication and epigenetic cell memory. Nat. Cell Biol. *22*, 361–371. https://doi.org/10.1038/s41556-020-0487-y.
4. Faundes, V., Newman, W.G., Bernardini, L., Canham, N., Clayton-Smith, J., Dallapiccola, B., Davies, S.J., Demos, M.K., Goldman, A., Gill, H., et al. (2018). Histone lysine methylases and demethylases in the landscape of human developmental disorders. Am. J. Hum. Genet. *102*, 175–187. https://doi.org/10.1016/j.ajhg.2017.11.013.
5. Kadoch, C., and Crabtree, G.R. (2015). Mammalian SWI/SNF chromatin remodeling complexes and cancer: mechanistic insights gained from human genomics. Sci. Adv. *1*, e1500447. https://doi.org/10.1126/sciadv.1500447.
6. Sokpor, G., Xie, Y., Rosenbusch, J., and Tuoc, T. (2017). Chromatin remodeling BAF (SWI/SNF) complexes in neural development and disorders. Front. Mol. Neurosci. *10*, 243. https://doi.org/10.3389/fnmol.2017.00243.
7. Ramachandran, S., and Henikoff, S. (2016). Transcriptional regulators compete with nucleosomes post-replication. Cell *165*, 580–592. https://doi.org/10.1016/j.cell.2016.02.062.
8. Stewart-Morgan, K.R., Reverón-Gómez, N., and Groth, A. (2019). Transcription restart establishes chromatin accessibility after DNA replication. Mol. Cell *75*, 284–297.e6. https://doi.org/10.1016/j.molcel.2019.04.033.
9. Annunziato, A.T. (2015). The fork in the road: histone partitioning during DNA replication. Genes *6*, 353–371. https://doi.org/10.3390/genes6020353.
10. Alabert, C., Barth, T.K., Reverón-Gómez, N., Sidoli, S., Schmidt, A., Jensen, O.N., Imhof, A., and Groth, A. (2015). Two distinct modes for propagation of histone PTMs across the cell cycle. Genes Dev. *29*, 585–590. https://doi.org/10.1101/gad.256354.114.
11. Jansen, L.E.T., Black, B.E., Foltz, D.R., and Cleveland, D.W. (2007). Propagation of centromeric chromatin requires exit from mitosis. J. Cell Biol. *176*, 795–805. https://doi.org/10.1083/jcb.200701066.
12. Reverón-Gómez, N., González-Aguilera, C., Stewart-Morgan, K.R., Petryk, N., Flury, V., Graziano, S., Johansen, J.V., Jakobsen, J.S., Alabert,

C., and Groth, A. (2018). Accurate recycling of parental histones reproduces the histone modification landscape during DNA replication. Mol. Cell *72*, 239–249.e5. https://doi.org/10.1016/j.molcel.2018.08.010.

13. Maison, C., Quivy, J.P., Probst, A.V., and Almouzni, G. (2010). Heterochromatin at mouse pericentromeres: a model for de novo heterochromatin formation and duplication during replication. Cold Spring Harb. Symp. Quant. Biol. *75*, 155–165. https://doi.org/10.1101/sqb.2010.75.013.
14. Marzluff, W.F., and Koreski, K.P. (2017). Birth and death of histone mRNAs. Trends Genet. *33*, 745–759. https://doi.org/10.1016/j.tig.2017.07.014.
15. Lanzuolo, C., Lo Sardo, F., and Orlando, V. (2012). Concerted epigenetic signatures inheritance at PcG targets through replication. Cell Cycle *11*, 1296–1300. https://doi.org/10.4161/cc.19710.
16. Petruk, S., Black, K.L., Kovermann, S.K., Brock, H.W., and Mazo, A. (2013). Stepwise histone modifications are mediated by multiple enzymes that rapidly associate with nascent DNA during replication. Nat. Commun. *4*, 2841. https://doi.org/10.1038/ncomms3841.
17. Alabert, C., Bukowski-Wills, J.C., Lee, S.B., Kustatscher, G., Nakamura, K., de Lima Alves, F., Menard, P., Mejlvang, J., Rappsilber, J., and Groth, A. (2014). Nascent chromatin capture proteomics determines chromatin dynamics during DNA replication and identifies unknown fork components. Nat. Cell Biol. *16*, 281–293. https://doi.org/10.1038/ncb2918.
18. Sirbu, B.M., McDonald, W.H., Dungrawala, H., Badu-Nkansah, A., Kavanaugh, G.M., Chen, Y., Tabb, D.L., and Cortez, D. (2013). Identification of proteins at active, stalled, and collapsed replication forks using isolation of proteins on nascent DNA (iPOND) coupled with mass spectrometry. J. Biol. Chem. *288*, 31458–31467. https://doi.org/10.1074/jbc.M113.511337.
19. Sirbu, B.M., Couch, F.B., and Cortez, D. (2012). Monitoring the spatiotemporal dynamics of proteins at replication forks and in assembled chromatin using isolation of proteins on nascent DNA. Nat. Protoc. *7*, 594–605. https://doi.org/10.1038/nprot.2012.010.
20. Thompson, A., Schäfer, J., Kuhn, K., Kienle, S., Schwarz, J., Schmidt, G., Neumann, T., Johnstone, R., Mohammed, A.K.A., and Hamon, C. (2003). Tandem mass tags: a novel quantification strategy for comparative analysis of complex protein mixtures by MS/MS. Anal. Chem. *75*, 1895–1904. https://doi.org/10.1021/ac0262560.
21. Sugimoto, N., and Fujita, M. (2017). Molecular mechanism for chromatin regulation during MCM loading in mammalian cells. Adv. Exp. Med. Biol. *1042*, 61–78. https://doi.org/10.1007/978-981-10-6955-0_3.
22. Ginno, P.A., Burger, L., Seebacher, J., Iesmantavicius, V., and Schübeler, D. (2018). Cell cycle-resolved chromatin proteomics reveals the extent of mitotic preservation of the genomic regulatory landscape. Nat. Commun. *9*, 4048. https://doi.org/10.1038/s41467-018-06007-5.
23. Lovering, R.C., Gaudet, P., Acencio, M.L., Ignatchenko, A., Jolma, A., Fornes, O., Kuiper, M., Kulakovskiy, I.V., Lægreid, A., Martin, M.J., and Logie, C. (2021). A GO catalogue of human DNA-binding transcription factors. Biochim. Biophys. Acta. Gene Regul. Mech. *1864*, 194765. https://doi.org/10.1016/j.bbagrm.2021.194765.
24. Berest, I., Arnold, C., Reyes-Palomares, A., Palla, G., Rasmussen, K.D., Giles, H., Bruch, P.M., Huber, W., Dietrich, S., Helin, K., and Zaugg, J.B. (2019). Quantification of differential transcription factor activity and multiomics-based classification into activators and repressors: diffTF. Cell Rep. *29*, 3147–3159.e12. https://doi.org/10.1016/j.celrep.2019.10.106.
25. Yin, Y., Morgunova, E., Jolma, A., Kaasinen, E., Sahu, B., Khund-Sayeed, S., Das, P.K., Kivioja, T., Dave, K., Zhong, F., et al. (2017). Impact of cytosine methylation on DNA binding specificities of human transcription factors. Science *356*, eaaj2239. https://doi.org/10.1126/science.aaj2239.
26. Festuccia, N., Gonzalez, I., Owens, N., and Navarro, P. (2017). Mitotic bookmarking in development and stem cells. Development *144*, 3633–3645. https://doi.org/10.1242/dev.146522.
27. Sherwood, R.I., Hashimoto, T., O'Donnell, C.W., Lewis, S., Barkal, A.A., van Hoff, J.P., Karun, V., Jaakkola, T., and Gifford, D.K. (2014). Discovery of directional and nondirectional pioneer transcription factors by modeling DNase profile magnitude and shape. Nat. Biotechnol. *32*, 171–178. https://doi.org/10.1038/nbt.2798.
28. Becker, J.S., McCarthy, R.L., Sidoli, S., Donahue, G., Kaeding, K.E., He, Z., Lin, S., Garcia, B.A., and Zaret, K.S. (2017). Genomic and proteomic resolution of heterochromatin and its restriction of alternate fate genes. Mol. Cell *68*, 1023–1037.e15. https://doi.org/10.1016/j.molcel.2017.11.030.
29. Fortuny, A., and Polo, S.E. (2018). The response to DNA damage in heterochromatin domains. Chromosoma *127*, 291–300. https://doi.org/10.1007/s00412-018-0669-6.
30. Llères, D., Bailly, A.P., Perrin, A., Norman, D.G., Xirodimas, D.P., and Feil, R. (2017). Quantitative FLIM-FRET microscopy to monitor nanoscale chromatin compaction in vivo reveals structural roles of condensin complexes. Cell Rep. *18*, 1791–1803. https://doi.org/10.1016/j.celrep.2017.01.043.
31. Vouzas, A.E., and Gilbert, D.M. (2021). Mammalian DNA replication timing. Cold Spring Harb. Perspect. Biol. *13*, a040162. https://doi.org/10.1101/cshperspect.a040162.
32. Samejima, I., Spanos, C., Samejima, K., Rappsilber, J., Kustatscher, G., and Earnshaw, W.C. (2022). Mapping the invisible chromatin transactions of prophase chromosome remodeling. Mol. Cell *82*, 696–708.e4. https://doi.org/10.1016/j.molcel.2021.12.039.
33. Blow, J.J., and Dutta, A. (2005). Preventing re-replication of chromosomal DNA. Nat. Rev. Mol. Cell Biol. *6*, 476–486. https://doi.org/10.1038/nrm1663.
34. Ly, T., Endo, A., and Lamond, A.I. (2015). Proteomic analysis of the response to cell cycle arrests in human myeloid leukemia cells. Elife *4*, e04534. https://doi.org/10.7554/eLife.04534.
35. Højfeldt, J.W., Laugesen, A., Willumsen, B.M., Damhofer, H., Hedehus, L., Tvardovskiy, A., Mohammad, F., Jensen, O.N., and Helin, K. (2018). Accurate H3K27 methylation can be established de novo by SUZ12-directed PRC2. Nat. Struct. Mol. Biol. *25*, 225–232. https://doi.org/10.1038/s41594-018-0036-6.
36. Blackledge, N.P., and Klose, R.J. (2021). The molecular principles of gene regulation by Polycomb repressive complexes. Nat. Rev. Mol. Cell Biol. *22*, 815–833. https://doi.org/10.1038/s41580-021-00398-y.
37. Gutierrez-Escribano, P., Hormeño, S., Madariaga-Marcos, J., Solé-Soler, R., O'Reilly, F.J., Morris, K., Aicart-Ramos, C., Aramayo, R., Montoya, A., Kramer, H., et al. (2020). Purified smc5/6 complex exhibits DNA substrate recognition and compaction. Mol. Cell *80*, 1039–1054.e6. https://doi.org/10.1016/j.molcel.2020.11.012.
38. Peters, J.M., and Nishiyama, T. (2012). Sister chromatid cohesion. Cold Spring Harb. Perspect. Biol. *4*, a011130. https://doi.org/10.1101/cshperspect.a011130.
39. Davidson, I.F., and Peters, J.M. (2021). Genome folding through loop extrusion by SMC complexes. Nat. Rev. Mol. Cell Biol. *22*, 445–464. https://doi.org/10.1038/s41580-021-00349-7.
40. Sima, J., Chakraborty, A., Dileep, V., Michalski, M., Klein, K.N., Holcomb, N.P., Turner, J.L., Paulsen, M.T., Rivera-Mulia, J.C., Trevilla-Garcia, C., et al. (2019). Identifying cis elements for spatiotemporal control of mammalian DNA replication. Cell *176*, 816–830.e18. https://doi.org/10.1016/j.cell.2018.11.036.
41. Busslinger, G.A., Stocsits, R.R., van der Lelij, P., Axelsson, E., Tedeschi, A., Galjart, N., and Peters, J.M. (2017). Cohesin is positioned in mammalian genomes by transcription, CTCF and Wapl. Nature *544*, 503–507. https://doi.org/10.1038/nature22063.
42. Karemaker, I.D., and Baubec, T. (2020). DNA methyltransferases hitchhiking on chromatin. Swiss Med. Wkly. *150*, w20329. https://doi.org/10.4414/smw.2020.20329.
43. Salhab, A., Nordström, K., Gasparoni, G., Kattler, K., Ebert, P., Ramirez, F., Arrigoni, L., Müller, F., Polansky, J.K., Cadenas, C., et al. (2018). A comprehensive analysis of 195 DNA methylomes reveals shared and cell-specific features of partially methylated domains. Genome Biol. *19*, 150. https://doi.org/10.1186/s13059-018-1510-5.

44. Hammond, C.M., Strømme, C.B., Huang, H., Patel, D.J., and Groth, A. (2017). Histone chaperone networks shaping chromatin function. Nat. Rev. Mol. Cell Biol. *18*, 141–158. https://doi.org/10.1038/nrm.2016.159.

45. Escobar, T.M., Yu, J.R., Liu, S., Lucero, K., Vasilyev, N., Nudler, E., and Reinberg, D. (2022). Inheritance of repressed chromatin domains during S phase requires the histone chaperone NPM1. Sci. Adv. *8*, eabm3945. https://doi.org/10.1126/sciadv.abm3945.

46. Voon, H.P.J., and Wong, L.H. (2016). New players in heterochromatin silencing: histone variant H3.3 and the ATRX/DAXX chaperone. Nucleic Acids Res. *44*, 1496–1501. https://doi.org/10.1093/nar/gkw012.

47. Wade, J.T., and Grainger, D.C. (2018). Spurious transcription and its impact on cell function. Transcription *9*, 182–189. https://doi.org/10.1080/21541264.2017.1381794.

48. Saredi, G., Huang, H., Hammond, C.M., Alabert, C., Bekker-Jensen, S., Forne, I., Reverón-Gómez, N., Foster, B.M., Mlejnkova, L., Bartke, T., et al. (2016). H4K20me0 marks post-replicative chromatin and recruits the TONSL-MMS22L DNA repair complex. Nature *534*, 714–718. https://doi.org/10.1038/nature18312.

49. Padeken, J., Methot, S.P., and Gasser, S.M. (2022). Establishment of H3K9-methylated heterochromatin and its functions in tissue differentiation and maintenance. Nat. Rev. Mol. Cell Biol. *23*, 623–640. https://doi.org/10.1038/s41580-022-00483-w.

50. Morgan, M.A.J., and Shilatifard, A. (2020). Reevaluating the roles of histone-modifying enzymes and their associated chromatin modifications in transcriptional regulation. Nat. Genet. *52*, 1271–1281. https://doi.org/10.1038/s41588-020-00736-4.

51. Agudelo Garcia, P.A., Hoover, M.E., Zhang, P., Nagarajan, P., Freitas, M.A., and Parthun, M.R. (2017). Identification of multiple roles for histone acetyltransferase 1 in replication-coupled chromatin assembly. Nucleic Acids Res. *45*, 9319–9335. https://doi.org/10.1093/nar/gkx545.

52. Lazarchuk, P., Hernandez-Villanueva, J., Pavlova, M.N., Federation, A., MacCoss, M., and Sidorova, J.M. (2020). Mutual balance of histone deacetylases 1 and 2 and the acetyl reader ATAD2 regulates the level of acetylation of histone H4 on nascent chromatin of human cells. Mol. Cell Biol. *40*, 00421-19. https://doi.org/10.1128/MCB.00421-19.

53. Olivieri, M., Cho, T., Álvarez-Quilón, A., Li, K., Schellenberg, M.J., Zimmermann, M., Hustedt, N., Rossi, S.E., Adam, S., Melo, H., et al. (2020). A genetic map of the response to DNA damage in human cells. Cell *182*, 481–496.e21. https://doi.org/10.1016/j.cell.2020.05.040.

54. Supek, F., and Lehner, B. (2015). Differential DNA mismatch repair underlies mutation rate variation across the human genome. Nature *521*, 81–84. https://doi.org/10.1038/nature14173.

55. Thompson, E.L., Yeo, J.E., Lee, E.A., Kan, Y., Raghunandan, M., Wiek, C., Hanenberg, H., Schärer, O.D., Hendrickson, E.A., and Sobeck, A. (2017). FANCI and FANCD2 have common as well as independent functions during the cellular replication stress response. Nucleic Acids Res. *45*, 11837–11857. https://doi.org/10.1093/nar/gkx847.

56. Tachibana, M., Sugimoto, K., Nozaki, M., Ueda, J., Ohta, T., Ohki, M., Fukuda, M., Takeda, N., Niida, H., Kato, H., and Shinkai, Y. (2002). G9a histone methyltransferase plays a dominant role in euchromatic histone H3 lysine 9 methylation and is essential for early embryogenesis. Genes Dev. *16*, 1779–1791. https://doi.org/10.1101/gad.989402.

57. Djeghloul, D., Patel, B., Kramer, H., Dimond, A., Whilding, C., Brown, K., Kohler, A.C., Feytout, A., Veland, N., Elliott, J., et al. (2020). Identifying proteins bound to native mitotic ESC chromosomes reveals chromatin repressors are important for compaction. Nat. Commun. *11*, 4118. https://doi.org/10.1038/s41467-020-17823-z.

58. Baubec, T., Colombo, D.F., Wirbelauer, C., Schmidt, J., Burger, L., Krebs, A.R., Akalin, A., and Schübeler, D. (2015). Genomic profiling of DNA methyltransferases reveals a role for DNMT3B in genic methylation. Nature *520*, 243–247. https://doi.org/10.1038/nature14176.

59. Sneppen, K., and Ringrose, L. (2019). Theoretical analysis of Polycomb-Trithorax systems predicts that poised chromatin is bistable and not bivalent. Nat. Commun. *10*, 2133. https://doi.org/10.1038/s41467-019-10130-2.

60. Tsubouchi, T., Soza-Ried, J., Brown, K., Piccolo, F.M., Cantone, I., Landeira, D., Bagci, H., Hochegger, H., Merkenschlager, M., and Fisher, A.G. (2013). DNA synthesis is required for reprogramming mediated by stem cell fusion. Cell *152*, 873–883. https://doi.org/10.1016/j.cell.2013.01.012.

61. Nakatani, T., Lin, J., Ji, F., Ettinger, A., Pontabry, J., Tokoro, M., Altamirano-Pacheco, L., Fiorentino, J., Mahammadov, E., Hatano, Y., et al. (2022). DNA replication fork speed underlies cell fate changes and promotes reprogramming. Nat. Genet. *54*, 318–327. https://doi.org/10.1038/s41588-022-01023-0.

62. Festuccia, N., Owens, N., Papadopoulou, T., Gonzalez, I., Tachtsidi, A., Vandoermel-Pournin, S., Gallego, E., Gutierrez, N., Dubois, A., Cohen-Tannoudji, M., and Navarro, P. (2019). Transcription factor activity and nucleosome organization in mitosis. Genome Res. *29*, 250–260. https://doi.org/10.1101/gr.243048.118.

63. Gonzalez, I., Molliex, A., and Navarro, P. (2021). Mitotic memories of gene activity. Curr. Opin. Cell Biol. *69*, 41–47. https://doi.org/10.1016/j.ceb.2020.12.009.

64. Sarkies, P., Reams, C., Simpson, L.J., and Sale, J.E. (2010). Epigenetic instability due to defective replication of structured DNA. Mol. Cell *40*, 703–713. https://doi.org/10.1016/j.molcel.2010.11.009.

65. Schneider, C.A., Rasband, W.S., and Eliceiri, K.W. (2012). NIH Image to ImageJ: 25 years of image analysis. Nat. Methods *9*, 671–675. https://doi.org/10.1038/nmeth.2089.

66. Tyanova, S., Temu, T., Sinitcyn, P., Carlson, A., Hein, M.Y., Geiger, T., Mann, M., and Cox, J. (2016). The Perseus computational platform for comprehensive analysis of (prote)omics data. Nat. Methods *13*, 731–740. https://doi.org/10.1038/nmeth.3901.

67. Raudvere, U., Kolberg, L., Kuzmin, I., Arak, T., Adler, P., Peterson, H., and Vilo, J. (2019). g:Profiler: a web server for functional enrichment analysis and conversions of gene lists (2019 update). Nucleic Acids Res. *47*, W191–W198. https://doi.org/10.1093/nar/gkz369.

68. Hughes, C.S., Foehr, S., Garfield, D.A., Furlong, E.E., Steinmetz, L.M., and Krijgsveld, J. (2014). Ultrasensitive proteome analysis using paramagnetic bead technology. Mol. Syst. Biol. *10*, 757. https://doi.org/10.15252/msb.20145625.

69. Brenes, A., Hukelmann, J., Bensaddek, D., and Lamond, A.I. (2019). Multibatch TMT reveals false positives, batch effects and missing values. Mol. Cell. Proteomics *18*, 1967–1980. https://doi.org/10.1074/mcp.RA119.001472.

70. Cox, J., and Mann, M. (2011). Quantitative, high-resolution proteomics for data-driven systems biology. Annu. Rev. Biochem. *80*, 273–299. https://doi.org/10.1146/annurev-biochem-061308-093216.

71. Kustatscher, G., Hégarat, N., Wills, K.L.H., Furlan, C., Bukowski-Wills, J.C., Hochegger, H., and Rappsilber, J. (2014). Proteomics of a fuzzy organelle: interphase chromatin. EMBO J. *33*, 648–664. https://doi.org/10.1002/embj.201387614.

STAR★METHODS

KEY RESOURCES TABLE

REAGENT or RESOURCE	SOURCE	IDENTIFIER
Antibodies		
Mouse Anti-PCNA Monoclonal Antibody, Unconjugated, Clone PC10	Abcam	Cat#ab29; RRID:AB_303394
Anti-Histone H3 antibody [mAbcam 10799]-ChIP Grade	Abcam	Cat#ab10799; RRID:AB_470239
Anti-Histone H4, pan, clone 62-141-13 antibody	Millipore	Cat#05-858; RRID:AB_390138
Anti-acetyl-Histone H4 (Lys12) Antibody	Millipore	Cat#07-595; RRID:AB_310740
Cdc6 (180.2)	Santa Cruz Biotechnology	Cat#sc-9964; RRID:AB_627236
Anti- MCM3 antibody	Abcam	Cat#ab4460; RRID:AB_304469
Anti-MCM2 antibody	Abcam	Cat#ab4461; RRID:AB_304470
Anti-Biotin Vector Laboratories	Vector Laboratories	Cat#SP-3000; RRID:AB_2336111
G9a/EHMT2 (C6H3)	Cell Signaling Technology	Cat#3306; RRID:AB_2097647
ATAD2 antibody, 23894-1-AP	Proteintech	Cat#23894-1-AP; RRID:AB_2879352
FANCD2 antibody [EPR2302]	Abcam	Cat#ab108928; RRID:AB_10862535
Tri-Methyl-Histone H3 (Lys27) (C36B11)	Cell Signaling Technology	Cat#9733; RRID:AB_2616029
Phospho-Histone H3 (Ser10) Antibody	Cell Signaling Technology	Cat# 9701; RRID:AB_331535
Peroxidase-AffiniPure Donkey Anti-Rabbit IgG (H + L) antibody	Jackson ImmunoResearch Labs	Cat#711-035-152; RRID:AB_10015282
Peroxidase-AffiniPure Goat Anti-Mouse IgG (H + L)	Jackson ImmunoResearch Labs	Cat#115-035-062; RRID:AB_2338504
anti-Rabbit IgG AF488	Invitrogen	Cat#1910751
Goat Anti-Mouse IgG (H + L), Alexa Fluor 546	Invitrogen	Cat# A11030; RRID:AB_144695
Chemicals, peptides, and recombinant proteins		
5-ethynyl-2′-deoxyuridine (EdU)	Thermo Fisher Scientific Inc.	Cat# E10187
Streptavidin-coated magnetic beads	Thermo Fisher Scientific Inc.	Cat# 65001
Azide-biotin	Thermo Fisher Scientific Inc.	Cat# B10184
Triptolide	Sigma	Cat# T3652
Mitomycin-C	Duchefa Biochemie	Cat# M0133.0002
Nocodazole	Sigma	Cat# M1404
EPZ-6438	Stratech	Cat# A8221-APE
Critical commercial assays		
TMT10plex™ Isobaric Mass Tag Labeling Kit	Thermo Fisher Scientific Inc.	Cat# 90110
Click-iT® EdU Imaging Kit	Thermo Fisher Scientific Inc.	Cat# B10184
Duolink® In Situ Red Starter Kit Goat/Rabbit	Merk	Cat# DUO92105
Duolink™ In Situ PLA® Probe Anti-Goat PLUS	Merk	Cat# DUO92003
Duolink™ In Situ PLA® Probe Anti-Rabbit MINUS	Merk	Cat# DUO92005
Duolink™ In Situ Detection Reagents Green	Merk	Cat# DUO92014
Monarch® PCR & DNA Cleanup Kit	NEB	Cat #T1030
NEBNext Ultra II kit for Illumina sequencing	NEB	Cat #E7370L
Deposited data		
Histone PTMs mass spec data	Alabert et al.[10]	PRIDE: PXD001980
HeLa S3 NCC data in early, mid and late replicated regions coupled to TMT mass spec (3 replicates)	This study	PRIDE: PXD035489

(*Continued on next page*)

Continued

REAGENT or RESOURCE	SOURCE	IDENTIFIER
HeLa S3 NCC data in mid replicated regions with nocodazole treated sample coupled to TMT mass spec (3 replicates)	This study	PRIDE: PXD038113
HeLa S3 NCC data in late replicated regions with EPZ-6438 treated sample coupled to TMT mass spec (3 replicates)	This study	PRIDE: PXD038376
TIG-3 iPOND data in mid replicated regions coupled to TMT mass spec (5 replicates)	This study	PRIDE: PXD036236
Repli-seq	ENCODE Project Consortium, 2012	GEO: GSM923449
Repli-seq	This study	PRJNA910149
Experimental models: Cell lines		
HeLa S3	ATCC	RRID#CVCL_0058
TIG-3	JCRB Cell Bank	JCRB0506
Software and algorithms		
FlowJo v8 software	BD Bioscience	https://www.flowjo.com
ImageJ	Schneider et al.[65]	https://imagej.nih.gov/ij/
MaxQuant (v 1.6.10.43)	Tyanova et al.[66]	http://www.coxdocs.org/doku.php?id=maxquant:common:download_and_installation
Perseus (1.6.7.0)	Tyanova et al.[66]	https://maxquant.net/perseus/
R	N/A	https://cran.r-project.org/mirrors.html
Prism	GraphPad	https://www.graphpad.com/scientific-software/prism/
g:Profiler	Raudvere et al.[67]	https://biit.cs.ut.ee/gprofiler/gost
Other		
BD FACSCanto II flow cytometer	BD Biosciences	N/A
BD FACSDiva Software (BD Biosciences).	BD Biosciences	N/A
ScanR High Content Screening Microscopy (Olympus).	Thermo Fisher Scientific Inc.	N/A
Orbitrap Fusion™ Tribrid™ Mass Spectrometer	Thermo Fisher Scientific Inc.	N/A
UltiMate™ 3000 RSLCnano Liquid Chromatography System	Thermo Fisher Scientific Inc.	N/A

RESOURCE AVAILABILITY

Lead contact

Further information and requests for resources and reagents should be directed to and will be fulfilled by the lead contact, Constance Alabert (calabert@dundee.ac.uk).

Materials availability

This study did not generate new unique reagents.

Data and code availability

The mass spectrometry proteomics data have been deposited to the ProteomeXchange Consortium via the PRIDE partner repository and are publicly available as of the date of publication. Accession numbers are listed in the key resources table. The Repli-seq dataset have been deposited to the Sequence Read Archive (SRA) database and is publicly available as of the date of publication. Accession number is listed in the key resources table.

This paper analyses existing, publicly available data. These accession numbers for the datasets are listed in the key resources table.

This paper does not report original code.

Any additional information required to reanalyse the data reported in this paper is available from the lead contact upon request.

EXPERIMENTAL MODEL AND SUBJECT DETAILS

HeLa S3 (female) and TIG-3 (male) cell lines were cultured in Dulbecco's Modified Eagle's Medium (DMEM, Gibco) containing 10% FBS fetal bovine serum (FBS, Gibco) and 1% penicillin/streptomycin at 37°C in 5% CO2 and humid environment. For NCC and repli-seq experiments, HeLa S3 cells were cultured in suspension using spinner flasks at 0.8–1.2 × 10^6 cells/mL and diluted every 24 h. To perform PLA experiments, adherent HeLa S3 were used.

METHOD DETAILS

Cell synchronisation

Cells were synchronized at the G1/S border by single thymidine block (Sigma, 2 mM, 17 h) and released into fresh media containing deoxycytidine (Sigma, 24 μM) at 1 × 10^6 cells/mL.

Drug treatments

For NCC experiments, cells were treated with EPZ-6438 (Stratech, 20 μM), or Nocodazole (Sigma, 40 μM, 14 h). For PLA assays, cells were treated, when shown, with 1 μM Triptolide for 2 h, 25 μM Mitomycin-C for 2 h, or DMSO as negative controls. Their references are indicated in the key resources table.

Nascent chromatin capture

HeLa S3 cells growing in suspension were released from a 17h single thymidine block for 2 h (early S-phase), 3.5 h (mid S-phase) or 5.5 h (late S-phase) being washed twice with warm PBS. Newly synthesised DNA was labeled with 50 μM biotin-dUTP (IBA lifesciences) in hypotonic buffer (50 mM KCl, 10 mM HEPES) for 5 min at 37°C, and then supplemented with medium to allow the DNA labeling for 15 min. Cells were collected (Nascent chromatin) or chased for the indicated time (mature chromatin, G2, early G1 and late G1). At the indicated times, samples are fixed in 2% formaldehyde for 15 min and crosslinking was stopped by 1% glycine for 5 min. Nuclei were isolated in sucrose buffer (0.3 M sucrose, 10 mM HEPES-NaOH at pH 7.9, 1% Triton X-100, 2 mM MgOAc) by douncing and chromatin was solubilized by sonication in sonication buffer (10 mM HEPES-NaOH at pH 7.9, 100 mM NaCl, 2 mM EDTA pH 8, 1 mM EGTA pH 8, 0.2% SDS, 0.1% sodium sarkosyl, 1 mM PMSF) using a Bioruptor Plus sonicator for 24 cycles (30 s. ON/90 s off). The protein nuclear fraction is collected at this point to be analyzed together with the pull-downs. b-dUTP– labeled chromatin was purified on streptavidin-coated magnetic beads (65,001, Thermo Fischer) after diluting the sample in the sonication buffer without SDS to obtain a 0.1% of SDS. After an overnight incubation at 4°C, beads are washed 5 times with the washed buffer (10 mM HEPES-NaOH pH 7.9; 100 mM NaCl; 2 mM EDTA pH 8; 1 mM EGTA pH 8; 0.1% SDS, 1 mM PMSF). Total nuclear fractions and isolated chromatin were de-crosslinked by boiling for 40 min in LSB (50 mM Tris-HCl at pH 6.8, 100 mM DTT, 2% SDS, 8% glycerol). The protocol was previously described in.[17]

Isolation of proteins in nascent DNA (iPOND)

iPOND was performed as described[19]: 1.5 × 10^8 synchronised TIG-3 cells (per time point) were labeled with 20 μM EdU (Thermo Fisher) for 11 min. The thymidine chased sample were washed twice and subsequently further incubated in medium containing 20 μM thymidine for the indicated times. All samples were crosslinked with 1% formaldehyde (Sigma) for 15 min at RT followed by 5 min incubation with 0.125 M glycine to quench the formaldehyde. Afterward, cells were scraped from the plate (on ice), permeabilized in 0.25% Triton X-100 in PBS for 30 min at RT and washed with 0.5% BSA in PBS. To conjugate biotin to EdU-labeled DNA, click chemistry reactions were performed for 1.5 h in the dark (10 μM Biotin-azide, 10 mM Sodium ascorbate, 2 mM $CuSO_4$ in 1xPBS). Cells were lysed (1% SDS in 50 mM Tris, pH 8.0, protease inhibitor), sonicated (Bioruptor, Diagenode), the lysate diluted 1:1 (v/v) with cold PBS containing protease inhibitor, and streptavidin beads (Thermo Fisher) used to capture the biotin-conjugated DNA-protein complexes. At this point, the protein lysate is collected to be analyzed together with the iPOND pulldown. Captured complexes were washed extensively using lysis buffer and 1 M NaCl. The proteins were eluted under reducing conditions by boiling in 2X LSB sample buffer for 30 min.

Immunoblotting

De-crosslinked samples were subjected to SDS–PAGE separation on NuPAGE 4–12% gels (Invitrogen, NP0321) in MOPS. Proteins were transferred onto 0.2 μm pore size nitrocellulose membranes (GE Healthcare, 10,600,001) at 18 V for 1 h using Trans-Blot SD Semi-Dry Transfer Cell (Bio-Rad). Membranes were blocked in 5% skimmed milk in tris-buffer saline (TBS, 50 mM Tris, pH 7.5, 150 mM NaCl) supplemented with 0.1% Tween 20 (TBS-T) for 1 h. Incubations with primary and secondary antibodies were performed as recommended for each provider, dilution is detailed here: Anti-PCNA(1:1000), anti-histone H3 (1:1000), anti-histone H4 (1:500), anti-H4K12ac (1:1000), anti-cdc6 (1:100), anti-MCM3 (1:1000), anti-MCM2 (1:1000), phosphor-histone H3 (1:1000), anti-H3K27me3 (1:1000), rabbit-HRP (1:10,000), mouse-HRP (1:10,000). Signals from HRP-conjugated antibodies were revealed by chemiluminescence substrates Super Signal West Pico PLUS (Thermo Fisher, 34,580). Membranes were imaged using ChemiDoc XRS+ (Bio-Rad).

Flow cytometry

Sample preparation

Cells were harvested, washed with cold PBS and fixed with ice-cold 70% ethanol. Fixed cells were washed and incubated with propidium iodide (PI) solution (50 μg/mL PI, 50 μg/mL RNaseA, 0.1% Triton X-100 in PBS) for 30 min at room temperature (RT).

Data acquisition and analysis

Data were acquired using a BD FACSCanto II flow cytometer (BD Biosciences) coupled to BD FACSDiva Software (BD Biosciences). 10, 000 events per sample were recorded. Data analysis was performed using FlowJo v8 software (BD Bioscience).

Microscopy

Immunofluorescence

For quantitative image-based cytometry (QIBC), HeLa S3 cells were seeded at 10,000 cells per well in clear bottom black 96-well plates (Greiner). 24 h later cells were treated with 20 μM EdU for 10 min, pre-extracted with cold 0.5% Triton X-100 CSK buffer with protease inhibitors before fixation 20 min in 2% formaldehyde. For EdU detection, Alexa 647 was covalently linked to EdU using Click-iT EdU Imaging Kit (Thermo Fisher, B10184). Samples were blocked with BSA and primary and secondary antibody incubation are performed according to the manufacturer conditions as follow: anti-Biotin (1:1000), anti-EHMT2 (1:50), anti-ATAD2 (1:100), anti-FANCD2 (1:500), anti-rabbit IgG AF488 (1:1000), anti-mouse IgG (H + L) (1:1000), Alexa Fluor 546 (1:1000)

Proximal ligation assay (PLA)

Cells were treated as for QIBC, apart from using azide-biotin (Thermo Fisher) to covalently link to EdU using the other components of the same kit Click-iT EdU Imaging Kit. PLA between biotin and the protein of interest was performed according to manufacturer instructions, using the Duolink In Situ Red Starter Kit Goat/Rabbit (Merk, DUO92105) and its homologous bigger kits Duolink In Situ PLA Probe Anti-Goat PLUS, Duolink In Situ PLA Probe Anti-Rabbit MINUS and Duolink In Situ Detection Reagents Green. After PLA protocol, cells were stained with DAPI (Thermo, 62,248) for 10 min in PBS, washed and left with PBS until imaging. Images were taken and analyzed with ScanR High Content Screening Microscopy (Olympus).

Mass spectrometry

TMT MS. Tandem mass tag (TMT)-based MS for quantitative proteomics analysis

NCC samples were prepared using SP3 protocol for TMT labeling as described in.[68] In brief, protein samples were mixed with SP3 beads (1: 10) and digested with trypsin (1: 50, trypsin: protein). Equal amounts (100 μg) of each peptide sample were dried and dissolved in 100 μL 100 mM TEAB buffer. TMT labeling of each sample were followed by the TMT10plex Isobaric Mass Tag Labeling Kit (Thermo Fisher Scientific) manual. The TMT labeled peptide samples were further fractionated using offline high-pH reverse-phase (RP) chromatography, as previously described.[69] The 24 fractions were subsequently dried and the peptides re-dissolved in 5% formic acid and analyzed by nanoLC–MS/MS system as previously described[69] (Orbitrap Fusion Tribrid Mass Spectrometer (Thermo Fisher Scientific), equipped with an UltiMate 3000 RSLCnano Liquid Chromatography System). The MS data were analyzed using MaxQuant (v 1.6.10.43) and searched against Homo Sapiens database from Uniport (Swissport, January 2020).[70] The TMT quantification was set to reporter ion MS3 type with 10plex TMT (LOT: UH285228). Protein groups output table from MaxQuant was cleaned, filtered and median normalised with Perseus (1.6.7.0).[66] Because NCC involves formaldehyde crosslinking, non-chromatin proteins could be captured. Filtering the datasets *in silico* using the interphase chromatin probability score developed by ChEP and machine learning[71] did not affect the conclusions of our analysis.

Repli-seq protocol

HeLa S3 cells were synchronised at the G1/S border by single thymidine arrest as described before and released in S phase for 2 h (early S phase), 3.5 h (Mid-S phase) and 5.5 h (late S phase). $10x10^7$ cells were used per time point. DNA was labeled for 20 min with 20 uM EdU and washed with PBS containing 10 uM thymidine. Cells were resuspended in ice-cold 0.25% Triton X-/PBS at $1.25x10^7$ cells/mL and incubated at RT for 30 min. Samples were washed in ice-cold 0.5% BSA/PBS and resuspended in click-IT reaction (10 uM Biotin-azide, 10 mM Na Ascorbate, 1 mM CuSO4), using 0.5 mL per $1x10^7$ cells. The click-IT reaction was incubated at RT for 1 h. Samples were washed with ice-cold 0.5% BSA/PBS and PBS. Cells were sonicated in lysis buffer (50mM Tris HCl pH 8.0, 1% SDS) for 24 cycles (30 s. ON/90 s off) and spinned at max speed for 30 min 20 uL of Dynabeads per sample were added and incubated over-night at 4°C. Beads were washed 4 times with B&W buffer (10 mM Tris-HCl pH 7.5, 2 M NaCl, 1 mM EDTA, 0/1% Tween 20), twice with 0.05% Tween 20 in TE, once with 10 mM Tris-HCl ph 7.5 and resuspended in 100 uL EB buffer. To elute, samples were incubated in 50 ug/mL RNAse for 30 min at 37°C and 0.5% SDS and 1 mg/mL proteinase K over-night at 37°C and at 65°C at least 6 h. 100 uL of TE was added and DNA was purified following the Monarch PCR & DNA clean-up kit instructions. Library preparation was done following the instructions of the NEBNext Ultra II kit for Illumina sequencing. The pooled library was subjected to a dual size selection using Agencourt AMPure XP beads using 0.45x and 1.4x beads: sample to enrich for fragments between 180 bp and 800 bp. Multiplexed libraries were sequenced with 2x150 bp paired-end reads by Novogene (HK) with ~50 Mio reads for each sample.

QUANTIFICATION AND STATISTICAL ANALYSIS

Mass spec data

MaxQuant software was used for the identification of proteins.[70] For HeLa S3, the datasets were analyzed and filtered with Perseus. Only proteins identified in the six experiments and with one or more unique peptides were kept in the clustering analysis. The analysis of specific group of proteins includes proteins identified in at least 4 out of the 6 experiments. Potential contaminants and only identified by site proteins were removed from the list and data was median normalised. Volcano plots were generated in Perseus and visualised in GraphPrism. Percentages of enrichment of each protein were calculated in Excel and heatmaps made in GraphPrism. R was used to perform hierarchical clustering (k = 18), script available upon request. For TIG-3 cells, the quantification and statistical analysis was performed as described for the HeLa datasets, with two modifications. Proteins that were more abundant in the negative control (no EdU labeling, +ClickIT) compared to the 2 h mature sample (LateS) were removed from all time points since considered as background/non-specific. Furthermore, only proteins that are identified in at least 4/5 experiments as well as have one or more unique peptides were kept in the analysis. The datasets were median normalised, and the percentage of enrichment calculated as described before.

Gene Ontology analysis of biological process and cellular compartment, as well as Kyoto Encyclopedia of Genes and Genomes (KEGG) and Reactome analyses were performed using gProfiler. GraphPrism was used to visualise the results.

High throughput microscopy data

High throughput microscopy images were analyzed with ScanR analysis software and ImageJ. Data were visualised and statistically analyzed in Tableau and GraphPrism.

FACS data

FACS data analysis was performed using FlowJo v8 software (BD Bioscience).

Sequencing data

Fastq files were trimmed using Trim Galore 0.5.0 with default parameters. Sequence reads were aligned to the reference indexed GRCm38 genome including splice junctions and compared to ENCODE data available under number GSM923449.

Statistical analysis

For PLA data, all t tests applied were unpaired and two-sided using GraphPrism. Averages and standard deviation from all the graphs shown were calculated in GraphPrism or Excel and plotted with GraphPrism. Pearson correlations were performed with a confidence interval of 95% and two-tailed in GraphPrism. Principal Components Analysis were performed in GraphPrism with a 95% of percentile level and 1000 simulations.